Российская Академия Наук

РОССИЙСКАЯ АКАДЕМИЯ НАУК

ИНСТИТУТ ПРОБЛЕМ БЕЗОПАСНОГО РАЗВИТИЯ АТОМНОЙ ЭНЕРГЕТИКИ

RUSSIAN ACADEMY OF SCIENCES

NUCLEAR SAFETY INSTITUTE

Препринт ИБРАЭ № IBRAE-2000-08

Preprint IBRAE- 2000-08

M.S. Veshchunov, A.V. Berdyshev, V.I. Tarasov

DEVELOPMENT OF FISSION GAS BUBBLE MODELS FOR UO_2 FUEL IN FRAMEWORK OF MFPR CODE

Москва 2000

Moscow 2000

Вещунов М.С, Бердышев А.В., Тарасов В.И. РАЗРАБОТКА МОДЕЛЕЙ ПОВЕДЕНИЯ ВНУТРИЗЕРЕННЫХ ПУЗЫРЕЙ В UO_2 ТОПЛИВЕ В РАМКАХ КОДА MFPR. Препринт № IBRAE-2000-08. Москва: Институт проблем безопасного развития атомной энергетики РАН. Декабрь 2000. 38 с. Библиогр.: 44 назв.

Аннотация

С целью улучшения микроскопического описания поведения внутризеренных пузырей в UO_2 топливе разработаны и имплементированы в механистический код MFPR новые модели. В моделях исследуется влияние эффектов радиационного и теплового растворения атомов из внутри- и межзеренных пузырей в различных режимах работы топлива: стационарного облучения, переходных и послерадиационного отжига. Имплементация новых моделей в код позволяет существенно улучшить моделирование выхода газа и распухания топлива, а также соответствие предсказаний кода по сравнению с микроструктурными измерениями в различных экспериментах.

Veshchunov M.S., Berdyshev A.V., Tarasov V.I. DEVELOPMENT OF FISSION GAS BUBBLE MODELS FOR UO_2 FUEL IN FRAMEWORK OF MFPR CODE. Preprint IBRAE-2000-08. Moscow: Nuclear Safety Institute. December 2000. 38 p. — Refs.: 44 items.

Abstract

In order to improve the microscopic description of the fission gas behaviour in UO_2 fuel, the new models are developed and implemented in the mechanistic code MFPR. The models treat irradiation and thermal re-solution effects on intra- and intergranular bubbles under various conditions of UO_2 fuel operation: steady-state irradiation, transient and post-irradiation annealing. Implementation of the newly developed models in the MFPR code allows a significant improvement of code predictions with respect to gas release and fuel swelling, being also in a fair agreement with microstructure observations in various tests.

Development of Fission Gas Bubble Models for UO_2 Fuel in Framework of MFPR Code

M.S. Veshchunov, A.V. Berdyshev, V.I. Tarasov

Nuclear Safety Institute (IBRAE), Russian Academy of Sciences

B.Tul'skaya, 52, Moscow, 113191

phone: (095) 955 2618, fax: (095) 958 0040, e-mail: vms@ibrae.ac.ru

1. Introduction

In a recent paper on the theory of fission gas bubble evolution in irradiated UO_2 fuel [1] it was demonstrated that currently existing models and codes generally underestimate irradiation effects at temperatures below ≈ 1500°C and thermal effects at temperatures above ≈ 1500°C. In order to improve the microscopic description of the fission gas behaviour in accordance with recommendations of [1], the new models were further developed and implemented in the mechanistic code MFPR (Module for Fission Product Release) that is currently under development in collaboration between IBRAE (Moscow) and IPSN (Cadarache, France) [2].

This allowed a significant improvement of the code predictions with respect to gas release and fuel swelling under various conditions of UO_2 fuel operation: steady-state irradiation, transient and post-irradiation annealing. The improved MFPR code was extensively validated against various tests from the literature including either integral (release and swelling) or microscopic measurements (such as bubble size distribution in the grain and grain surface) at different temperatures, fission rates and burn-ups.

The description of the newly developed models, their implementation in the MFPR code and some results of code validation, are presented in the following sections.

2. Irradiation effects on intragranular bubbles in high-burnup fuel

Analysis [1] of intragranular bubbles behaviour shows that irradiation effects can produce strong limitations on the maximum bubble number density attained under steady irradiation conditions at temperatures below 1500° C. A new model that accounts for the irradiation induced limitation on the bubble sink strength in accordance with the recommendation of [1], is introduced in the MFPR code and described in the present Section 2. Results of numerical simulations with the new version of the MFPR code allows a satisfactory prediction of intragranular bubbles evolution at a late stage of irradiation observed in recent tests with high burn-up fuel.

2.1. Analysis of irradiation effects

As outlined in [1], essential parameters determining the intragranular bubble system behaviour under steady irradiation conditions in UO_2 fuel are the non-equilibrium point defect concentrations c_v (vacancies) and c_i (interstitials). For their calculation one can use the rate theory continuum model of Brailsford and Bullough [3]:

$$dc_v/dt = K + K_e - D_v c_v k_v^2 - \alpha D_i c_i c_v , \tag{2.1}$$

$$dc_i/dt = K - D_i c_i k_i^2 - \alpha D_i c_i c_v , \tag{2.1'}$$

where K is the atomic displacement rate, K_e is the rate of thermal vacancy production, $k_{v(i)}^2$ is the sink strength for vacancies (interstitials), α is the recombination constant ($\approx 4\pi r_c/\Omega$, where $r_c \approx 0.1$–0.5 nm [4]). Under the PWR reactor normal operation conditions $K = Fz_s\Omega$, where F is the fission rate, $z_s \approx (1–5)\times 10^5$ is

the damage formation in the fission track volume, $\Omega \approx 4.1\times10^{-23}$ cm^3 is the specific volume of the uranium atoms, thus, for the typical value $F = 10^{13}$ cm^{-3}s^{-1}, one can estimate $K \approx 10^{-5} - 10^{-4}$ s^{-1} [4].

If voids and dislocations are the only fixed sinks,

$$k_v^2 = 4\pi\rho_b R_b + Z_v\rho_d, \tag{2.2}$$

$$k_i^2 = 4\pi\rho_b R_b + Z_i\rho_d, \tag{2.2'}$$

where ρ_b and ρ_d are the void number and dislocation density, respectively; the dislocation sink strength constants Z_v and Z_i for vacancies and interstitials are the order of unity, but Z_i is a few percent larger due to the greater elastic interaction between dislocations and interstitials, than with vacancies [3].

In the steady state ($dc_v/dt = dc_i/dt = 0$) the general solution of Eqs. (2.1) is:

$$c_v = (k_i^2/2\alpha)[-(1-\mu) + ((1+\mu)^2 + \eta)^{1/2}], \tag{2.3}$$

$$c_i = (D_v k_v^2/2D_i\alpha)[-(1+\mu) + ((1+\mu)^2 + \eta)^{1/2}], \tag{2.3'}$$

where

$$\eta = 4\alpha K/(D_v k_i^2 k_v^2), \quad \mu = K_e\eta/(4K). \tag{2.4}$$

As demonstrated in [1], at $T < 1500^\circ$C $K_e << K$; on the other hand, η occurs to be rather large ($>> 1$) during a very long initial stage of the steady state period of irradiation. Indeed, at $T \approx 1000^\circ$C $D_v \approx 10^{-11} - 10^{-12}$ cm^2/s, and the relationship $\eta >> 1$ is valid until the parameters k_i^2, k_v^2 attain the value $\approx 10^{11} - 10^{12}$ cm^{-2}, i.e. practically up to the maximal observed number density of the bubbles (with $R_b \approx 1$ nm), $\rho_b \approx 10^{17} - 10^{18}$ cm^{-3}. At higher temperatures (up to 1500°C) this relationship is valid in a slightly reduced range of the parameters $k_{v,i}^2$ variation owing to some possible increase (within one order magnitude) of D_v. At lower temperatures (below 1000 °C) the uranium self-diffusion coefficient D_u becomes completely athermal and independent on temperature: $D_u \approx AF$, where $A \approx 1.2\times10^{-29}$ cm^5, thus, $D_u \approx 10^{-16}$ cm^2/s at the fission rate $F \approx 10^{13}$ cm^{-3}s^{-1}. As shown in [1], D_v becomes also temperature independent and, thus, the applicability range of the relationship $\eta >> 1$ does not reduce.

This is a rather important conclusion, since in this case the general solution, Eqs. (2.3) can be simplified:

$$c_v \approx (K\Omega k_i^4/4\pi r_c k_v^2 k_i^2 D_v)^{1/2} \approx (K\Omega/4\pi r_c D_v)^{1/2}, \tag{2.5}$$

$$D_i c_i \approx D_v c_v (k_v^2/k_i^2), \tag{2.5'}$$

i.e. c_v, c_i become practically independent on the amount of voids and dislocations in the crystal, since the mutual recombination of the point defects dominates in this stage. Owing to $D_u \approx D_v c_v \approx D_i c_i$, finally one gets:

$$c_v \approx K\Omega/4\pi r_c D_u, \tag{2.6}$$

$$D_v \approx 4\pi r_c D_u^2/K\Omega. \tag{2.7}$$

After completion of the "recombination stage", $\eta \le 1$ and dislocations and bubbles become the main sinks determining the steady state concentration of the point defects. As already mentioned, at $T < 1500^\circ$C the transition to the new regime occurs at a late stage of the steady irradiation, when the bubble number density attains $\rho_b \approx 10^{17} - 10^{18}$ cm^{-3}. In the new, "post-recombination stage" the general steady state solution, Eq. (2.3) can be reduced to the form:

$$c_v \approx K/k_v^2 D_v, \qquad \text{or} \qquad K \approx k_v^2 D_v c_v \approx k_v^2 D_u.$$

As already mentioned, at $T \le 1000^\circ C$ D_u depends only on the fission rate F and does not depend on temperature. At higher temperatures (up to $1500^\circ C$) D_u smoothly increases within one order of magnitude. Therefore, in the new regime k_v^2 attains the steady value:

$$k_v^2 \approx K/D_u \approx z_s \Omega/A. \tag{2.8}$$

This value weakly depends on temperature, being $k_v^2 \approx 10^{12}\,cm^{-2}$ at $T \le 1000^\circ C$ and possibly decreasing within one order of magnitude at $T \le 1500^\circ C$. Moreover, in all these cases k_v^2 corresponds to the maximum value attained in the recombination stage. Indeed, after substitution of Eq. (2.7) in Eq. (2.4) one can see that the calculated in Eq. (2.8) value $k_v^2 = K/D_u$ determines the upper limit of the recombination stage providing $\eta = 1$. This means that the maximum value of k_v^2 attained at $T \le 1500^\circ C$ in the recombination stage is practically final and does not increase anymore during the subsequent stage.

This prediction is in a remarkable agreement with experimental observations [5, 6]. In these tests the detailed characteristics of intragranular bubbles and dislocations in UO_2 fuel pellets in a wide range of burnups 6 – 83 GWd/t were examined by TEM and SEM fractography. From the measured values of the bubble number density, mean bubble diameter and dislocation density, one can evaluate the sink strengths of the dislocation and intragranular bubble subsystems. In accordance with this evaluation, $4\pi\rho_b R_b >> Z_{i,v}\rho_d$ and the total sink strength $k_v^2 \approx 4\pi\rho_b R_b$ attains the maximum value $k_v^2 \approx (1–1.5)\cdot 10^{12}\ cm^{-2}$ at burn-up 23 GWd/t and remains practically invariable at higher burn-ups up to 83 GWd/t, in agreement with the model prediction, Eq. (2.8).

On the other hand, such a behaviour of the bubble system contradicts to the calculations by the previous version of the MFPR code, which predicts that the value of $4\pi\rho_b R_b$ continuously grows up with the irradiation dose increase, Fig. 2.1, and can considerably exceeds the limiting value following from theoretical [1] and experimental [5, 6] considerations.

2.2. Model description

In order to self-consistently eliminate this code deficiency, an additional microscopic consideration within the MFPR code of the non-equilibrium point defect subsystem and its interaction with bubble and dislocation subsystems is required, and may be the subject of the further code development. In the frame of the present approach, this problem is solved in a simplified manner. Namely, in the present version of the MFPR code the above derived limitation on the sink strength $k_v^2 = k_v^{2*} \approx 10^{12}\ cm^{-2}$ at the late ("post-recombination") stage of irradiation, is introduced in a phenomenological way.

Formally such a procedure is performed by multiplication of the nucleation probability F_n by the term:

$$\left(1 - \frac{4\pi\rho_b R_b}{k_v^{*2}}\right), \tag{2.9}$$

that provides the desired limitation to the bubbles sink strength at high irradiation doses (see Fig. 2.2) for the following reasons. At small values $4\pi\rho_b R_b << k_v^{*2} = 1.2\cdot 10^{12}\ cm^{-2}$ the factor from Eq. (2.9) is very close to unit and does not change nucleation probability, whereas at large values $4\pi\rho_b R_b >> 1.2\cdot 10^{12}\ cm^{-2}$ the corresponding term for bubble nucleation in the MFPR equations for evolution of gas and bubble subsystems

$$16\pi F_n R_g D_g C_g^2 \times \left(1 - \frac{4\pi\rho_b R_b}{k_v^{*2}}\right), \tag{2.10}$$

becomes negative with a very large absolute value. Eventually this suppresses further growth of the term $4\pi\rho_b R_b$ when the latter exceeds the limiting value k_v^{*2}. Application of a more steep function of the parameter

$\rho_b R_b$ in Eq. (2.10) instead of the linear function from Eq. (2.9), in order to reduce the "transition" interval between two areas of small and large values of $4\pi\rho_b R_b$, e.g.

$$f(x)=\begin{cases}1-\exp\left|100\left(1-\dfrac{4\pi\rho_b R_b}{k_v^{*2}}\right)\right|, & 4\pi\rho_b R_b \le (k_v^*)^2\\ -1+\exp\left|100\left(1-\dfrac{4\pi\rho_b R_b}{k_v^{*2}}\right)\right|, & 4\pi\rho_b R_b > (k_v^*)^2\end{cases},$$

provides practically the same evolution of the sink strength k_v^2 (as presented in Fig. 2.2), and for this reason the nucleation term in the simplest form, Eq. (2.10) was kept in the following calculations.

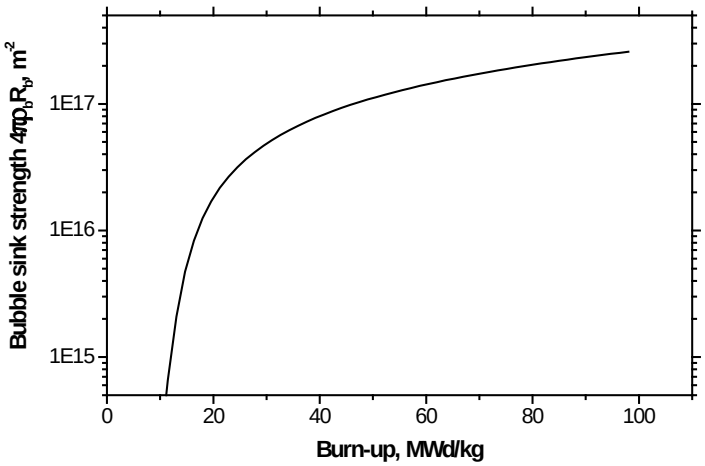

Fig. 2.1. Bubble sink strength as function of burn-up, calculated by the previous MFPR version.

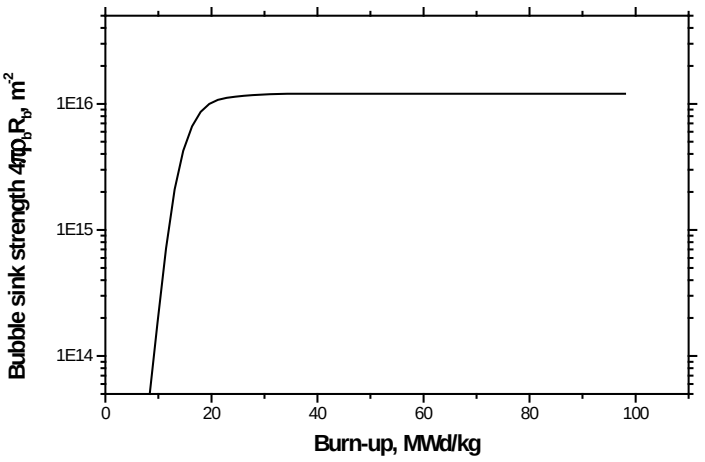

Fig. 2.2. The same as in Fig. 2.1 but calculated by the new MFPR version

2.3. Model validation

Results of validation of the new model against the experimental data [5, 6] are presented in Figs. 2.3 and 2.4. As one can see from Fig. 2.3, the calculated intragranular bubble diameter is in a qualitative agreement with observations, but approximately two times smaller then experimentally measured. This inconsistency is eliminated in calculations with the re-solution constant b reduced from $2 \cdot 10^{-23}$ to $5 \cdot 10^{-22}$ m^{-3} (see Figs. 2.5 and 2.6), in a qualitative correspondence with the new model for gas atom re-solution from large bubbles (with $R_b > 1.5$ nm) presented in the following Section 3.

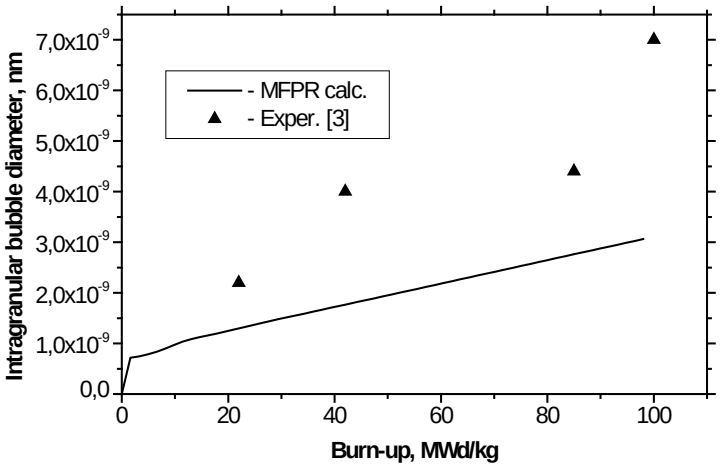

Fig. 2.3. Intragranular bubble diameter as a function of burn-up; resolution constant $b = 2 \cdot 10^{-23}$ m^{-3}.

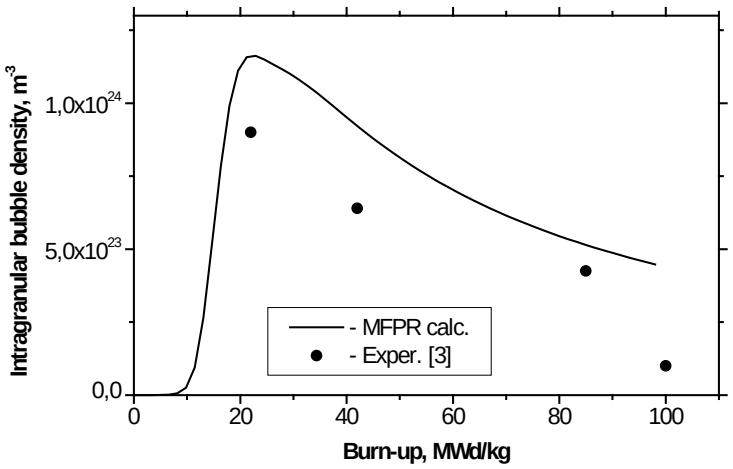

Fig. 2.4. Intragranular bubble number density as a function of burn-up; resolution constant $b = 2 \cdot 10^{-23}$ m^{-3}.

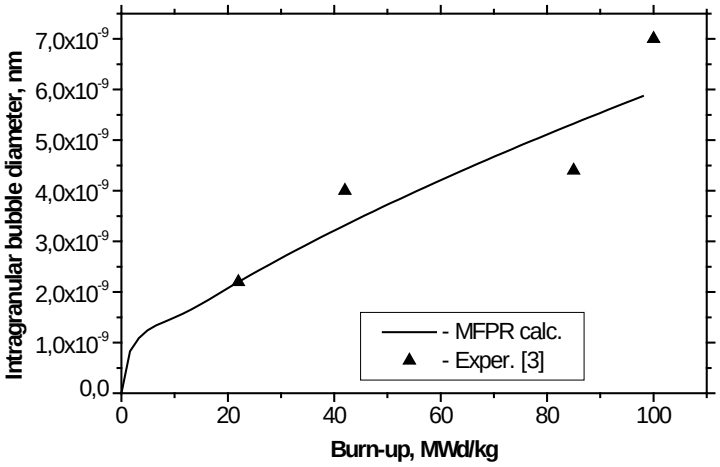

Fig. 2.5. Intragranular bubble diameter as a function of burn-up; resolution constant $b = 5 \cdot 10^{-22}\ m^{-3}$.

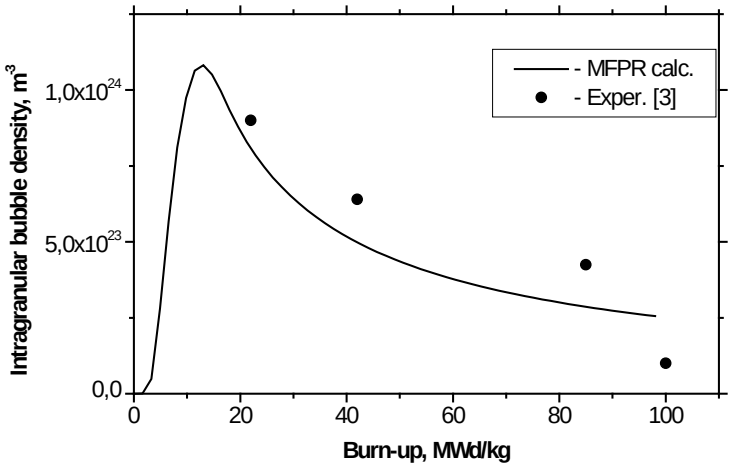

Fig. 2.6. Intragranular bubble number density as a function of burn-up; resolution constant $b = 5 \cdot 10^{-22}\ m^{-3}$.

2.4. Discussion

Despite the phenomenological nature of the presented approach, it allows the correct prediction of the bubbles behaviour at high burn-ups. However, it seems rather important to reproduce these results also in a more detailed microscopic model, in order to clarify physical processes responsible for the above described behaviour, for instance, in modelling of the microscopic mechanisms responsible for the formation of the so-called "rim structure" (associated with consolidation of dislocation structure in subgrain boundaries and subsequent growth of intergranular bubbles on these boundaries) observed at fuel periphery.

A similar procedure was recently attempted in the literature [7], however, technical mistakes (e.g. erroneous Eq. (6) in [7]) and inconsistencies (e.g. non-physically small values of model parameters such as the interstitial preference to dislocations, $(Z_i - Z_v)/Z_v = 10^{-3}$, etc.) probably prevents the authors [7] from the correct modelling.

For example, curves similar to Figs. 2.5 and 2.6 in the present report were reproduced in [7] only under additional assumptions for the nucleation factor $F_n = 1$ and re-solution factor $b = 0$, unacceptable for the mechanistic approach.

2.5. Conclusions

A new model that accounts for the irradiation induced limitation on the bubble sink strength at T < 1500°C under steady irradiation conditions, is introduced in the MFPR code. Results of numerical simulations with the new model allows a satisfactory prediction of a complicated non-monotonous behaviour of intragranular bubbles at a late stage of irradiation observed in recent tests with high burn-up fuel.

3. Irradiation effects on intragranular bubbles in transient tests

General analysis of the intragranular bubbles behaviour demonstrates that re-solution of gas atoms from bubbles is often treated in an oversimplified manner, and for this reason, additional studies of the irradiation effects on intragranular bubbles should be carried out.

Development of a new model for a self-consistent consideration of the irradiation induced re-solution of gas atoms from bubbles and its implementation in the MFPR code, are presented in the current Section 3. This allows a significant improvement in predictions for microscopic observations in the transient tests.

3.1. Advanced model for gas atoms re-solution from bubbles

According to the Nelson's model [8] for intragranular bubbles, the re-solution rate is independent of the bubble size only for very small bubbles ($R_b \leq$ 1–1.5 nm). For larger spherical bubbles only a fraction of gas atoms within a critical distance from the bubble surface $\lambda \approx$ 1–1.5 nm may escape, therefore, the resolution rate becomes inversely proportional to the bubble radius:

$$J_{res} = bN_b, \tag{3.1}$$

where

$$b \approx b_0\lambda/(\lambda + R_b), \tag{3.2}$$

is the resolution probability, and N_b is the number of atoms in a bubble. On the other hand, it was pointed out in [8] that for larger bubbles the ejection of a gas atom into surrounding matrix does not automatically result in its resolution. In accordance with available studies of the thermal desorption of inert gas from solids, it was presumed in [8] that those gas atoms knocked to within the first two or three atomic distances (i.e. $\delta \sim$ 1 nm) from the bubble would tend to return back to the bubble.

In order to take this tendency into quantitative consideration, one can assume that the influx of the ejected atoms back to the bubble proceeds by diffusion within the re-solution layer δ. Such a consideration generalises the standard treatment of the thermal re-solution of gas atoms from bubbles, and is similar to the consideration [9] of the re-solution process from grain boundaries. The built-up concentration barrier c_δ of the resolution layer determines the diffusion flux from the grain with the mean bulk concentration c_g of gas atoms in the matrix:

$$J_{dif} = 4\pi D(c_g - c_\delta)(R_b + \delta), \tag{3.3}$$

and the net flux of atoms deposited on the bubble:

$$J_\delta = 4\pi D c_\delta R_b(R_b + \delta)/\delta, \tag{3.4}$$

which counterbalances the re-solution flux J_{res} back into the grain in accordance with the flux matches:

$$J_{dif} + J_{res} = J_\delta. \tag{3.5}$$

Superposition of Eqs. (3.1–5) yields an equation for c_δ:

$$4\pi D c_\delta R_b (R_b + \delta)/\delta - bN_b = 4\pi D(c_g - c_\delta)(R_b + \delta). \quad (3.6)$$

Substitution of the solution of Eq. (3.6) in the equation for the growth rate of the bubble

$$dN_b/dt = J_{dif}, \quad (3.7)$$

yields:

$$dN_b/dt = 4\pi D c_g R_b - bN_b \cdot [\delta/(\delta + R_b)], \quad (3.8)$$

thus, leading to the additional re-normalisation of the re-solution probability b in the standard equation for the bubble growth rate (obtained disregarding the re-solution barrier c_δ).

Therefore, the self-consistent consideration of the gas atom re-solution from and influx back to bubbles allows application of the standard equation for the bubble growth rate:

$$dN_b/dt = 4\pi D c_g R_b - b' N_b , \quad (3.9)$$

however, with the following expression for the re-solution probability:

$$b' \approx b_0[\lambda/(\lambda + R_b)] \cdot [\delta/(\delta + R_b)]. \quad (3.10)$$

In the limiting case of a very large value of the re-solution layer thickness δ comparable with the inter-bubble distance, Eq. (3.10) transforms back into the Nelson's expression for b, Eq. (3.2). However, in accordance with the above mentioned Nelson's notification, this value is small and comparable with the value of λ, i.e. $\delta \sim \lambda \sim$ 1–1.5 nm, and for this reason, Eq. (3.10) will be further used in the simplified form:

$$b' \approx b_0[\lambda/(\lambda + R_b)]^2 . \quad (3.11)$$

On the other hand, strictly speaking Eq. (3.2) was derived in [8] for small bubbles with $R_b \le 5$ nm, i.e. for the Van-der-Waals bubbles with the gas density being effectively independent of bubble size. For larger bubbles the dependence of b on R_b may be slower, and Eq. (3.11) may be rewritten in a more general form:

$$b' \approx b_0[\lambda/(\lambda + R_b)]^\alpha , \quad (3.12)$$

with $1 \le \alpha \le 2$. In order to analyse the effect of superposition of the two power laws in the effective dependence of b' on R_b in Eq. (3.12), two limiting values $\alpha = 1$ and 2 corresponding to Eqs. (3.2) and (3.11), respectively, will be used in the following consideration.

3.2. Qualitative consideration

In order to analyse the bubble growth qualitatively, it is sufficient to consider the behaviour of a sole growing bubble during a time interval between two subsequent collisions with other bubbles [1]. Owing to a relatively low Brownian mobility of bubbles at $T \le 1800^\circ$C [10], the time between two subsequent collisions of a bubble (in the absence of temperature gradients in the grain) is really very large. In this case the analysis of the growing bubbles behaviour can be performed on the basis of Eq. (3.9) along with the kinetic equation for the number of vacancies x in a bubble, in terms of the phase portrait of the system, Fig. 3.1 (compare with [1]).

In the case of applicability of the ideal gas law (that is strictly valid for large bubbles with $R_b > 5$ nm) the first nodal line $dx/dt = 0$ is described by the "capillarity" equation $N \propto x^{2/3}$. The second nodal line $dN/dt = 0$ is represented by an equation $N \propto x^{1/3}$ for small bubbles with $R_b \le \lambda \sim 1$ nm, and by an equation $N \propto x^{2/3}$ for larger bubbles, if Eq. (3.2) is valid. In both these cases an intersection of the two nodal lines determines a unique critical point I of the stable node type, i.e. particles (gas atoms (N) and vacancies (x)) move toward the node from

all quadrants in the neighbourhood, Fig. 3.1. The critical point apparently determines the radius of the stable bubbles and explains the validity of the "bimodal" bubble size distribution, observed in the steady state tests. When a bubble deviates from this stable state, diffusion fluxes of the gas atoms and point defects arise which return the bubble back to the initial state. An account of the Brownian mobility of bubbles (increasing with temperature) may enlarge the mean size of bubbles, but will not change the situation qualitatively, since the system is still characterised by the unique stable critical point.

However, the situation can change when Eq. (3.11) is used instead of Eq. (3.2). In this case the nodal line $dN/dt = 0$ is described by a relationship $N \propto x$ for large bubbles $R_b >> \lambda$, and a new critical point of the saddle type appears at the intersection of the two nodal lines, Fig. 3.2. In the case of a sufficiently high bubble mobility (i.e. at high temperatures), bubbles can surmount the "distance" between the two critical points due to their collisions and coalescence, and thus "infiltrate" through the saddle point into the large-bubble area where they grow further unrestrictedly.

Therefore, under conditions of transient tests with temperature increase, the self-consistent consideration of the gas atom re-solution from and influx back to bubbles allows the prediction of the onset and growth of very large intragranular bubbles. This qualitatively corresponds to the observations in the transient tests [11, 12], and will be analysed quantitatively by application of the rapid dependence of re-solution probability b on bubble radius R_b derived in Eq. (3.11), in the following subsection.

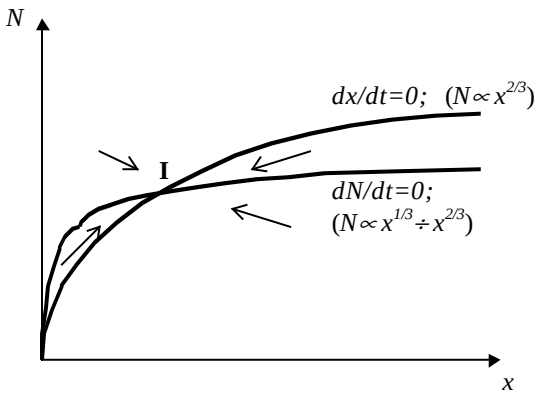

Fig. 3.1. Schematic diagram of nodal lines in the case of a slow dependence of b on R_b, i.e. $\alpha = 0 \div 1$. Velocity vectors and the critical point I *(stable node) are indicated .*

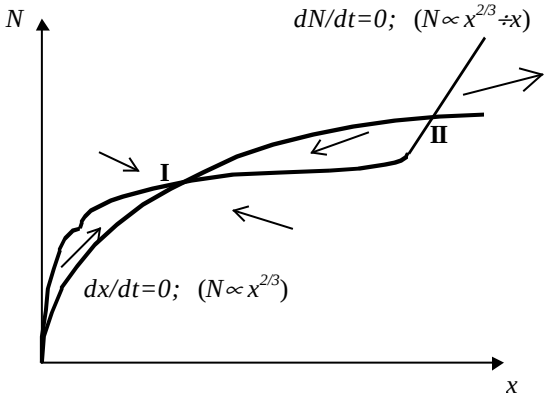

Fig. 3.2. Schematic diagram of nodal lines in the case of a rapid dependence of b on R_b, i.e. $\alpha = 1 \div 2$. Two critical points I *(stable node) and* II *(saddle) are indicated .*

3.3. Model validation

Transmission electron microscopy (TEM) has been used in an extensive study [11] of the microstructure of base-irradiated and transient-tested samples of LWR nuclear fuels. The steady state base irradiation of 3% enriched UO_2 fuel was performed at a maximum linear power of 260 W/cm (corresponding to the fission rate $\approx 1.3 \cdot 10^{13}$ fissions/s·cm^3) to an average burnup of 4.5%. The transient-tested samples came from pellets of the base-irradiated fuel which had been further subjected in reactor to power increases up to a maximum of 420 W/cm (fission rate $\approx 2.1 \cdot 10^{13}$ fissions/s·cm^3) with hold time up to 60 h (= $2.2 \cdot 10^5$ s).

Under steady-state irradiation conditions most of the fission gas produced was retained in solution in the fuel matrix or precipitated into small fission bubbles with a narrow size distribution and an average diameter of 8 nm. The bubble spatial distribution was homogeneous, with an average density of $(1.2–1.9) \cdot 10^{22}$ m^{-3}.

The effect of the transient test was to increase the fuel centre temperature from 1200°C by about 300°C, causing significant changes to fuel microstructure. The major microstructural change in the fuel centre resulting from the transient was the formation of a new population of large fission bubbles with a broad bubble size distribution (30 to 500 nm in diameter) and an average bubble density of 7×10^{18} m^{-3}. The temperature rise at the

fuel periphery, on the other hand, was small and the microstructure remained essentially similar to that of the base-irradiated fuel, with similar density and distribution of small fission bubbles.

Results of the standard MFPR version calculations of the transient tests [11] show that the increase of temperature from 1200 to 1500°C and fission rate from $1.3 \cdot 10^{13}$ to $2.1 \cdot 10^{13}$ fissions/s·cm^3 leads to an insignificant increase of the mean bubble diameter and the bubble distribution function width, however, conserves the bimodal character of this distribution (in accordance with qualitative predictions in Section 3.2), also at longer times after transient, Fig. 3.3. An agreement with observations might be improved only by a significant increase of the bubble mobility by several orders of magnitude (see Figs. 3.4 and 3.5 which demonstrate that a factor of 10^2 is still insufficient for the agreement), however, currently there are no physical reasons for such a tuning procedure.

Implementation in the MFPR code of the advanced model for gas re-solution from bubbles, Eq. (3.11), allows qualitative and quantitative improvement of the code predictions. Owing to the onset of the new critical point at the intersection of the two nodal lines in the phase portrait of the system, Fig. 3.2, and higher bubbles diffusivities at elevated temperatures, the formation of the "trimodal" bubble distribution function (i.e. single atoms and two populations of bubbles) with an extended interval of bubble sizes is predicted. Moreover, distribution function widens continuously with time after transient and becomes very similar to the observations [11], however, at somewhat longer times, Fig. 3.6. Increase of the bubble effective mobility allows further improvement of code predictions also at short times after transient, Fig. 3.7.

3.4. Conclusions

A new model for self-consistent consideration of the irradiation induced re-solution of gas atoms from bubbles is developed and implemented in the MFPR code. This allows to avoid (or to reduce) non-physical tuning of the code parameters (i.e. bubble diffusivity) and to attain a reasonable prediction for microscopic observations (i.e. bubble size distribution) in the transient tests.

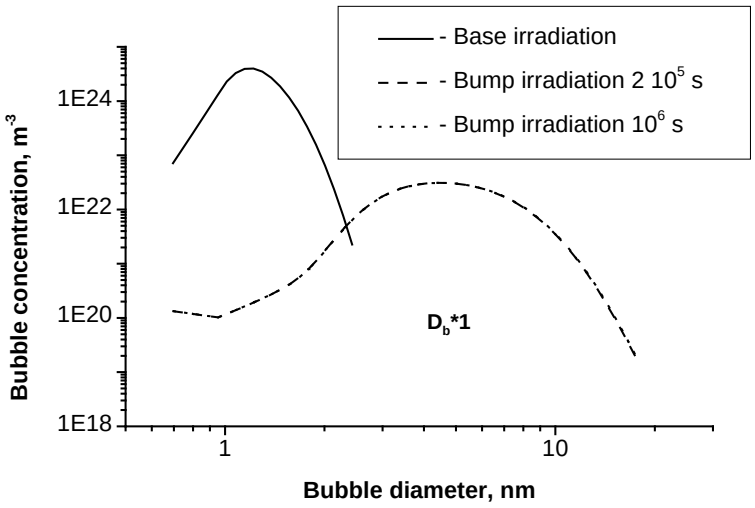

Fig. 3.3. Size distribution function of intragranular bubbles calculated by MFPR with standard model for gas re-solution from bubbles.

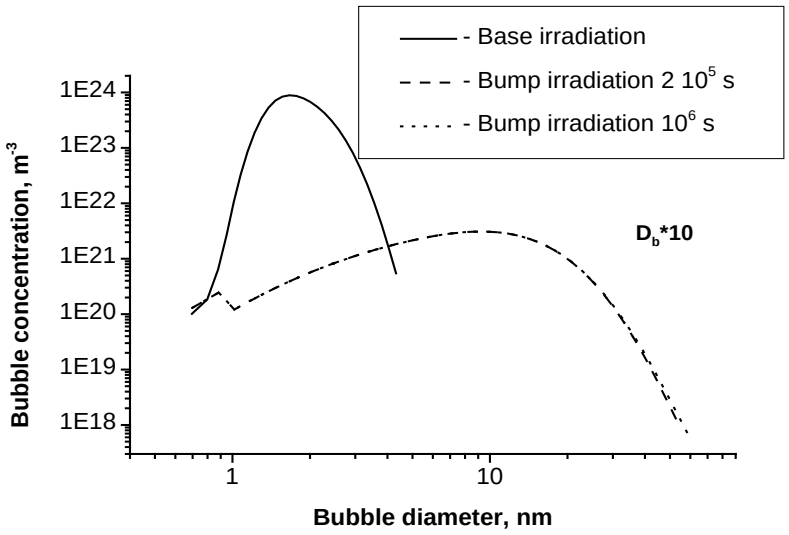

Fig. 3.4. Size distribution function of intragranular bubbles calculated by MFPR with standard model for gas re-solution from bubbles. Diffusion coefficient of bubbles is multiplied by a factor of 10.

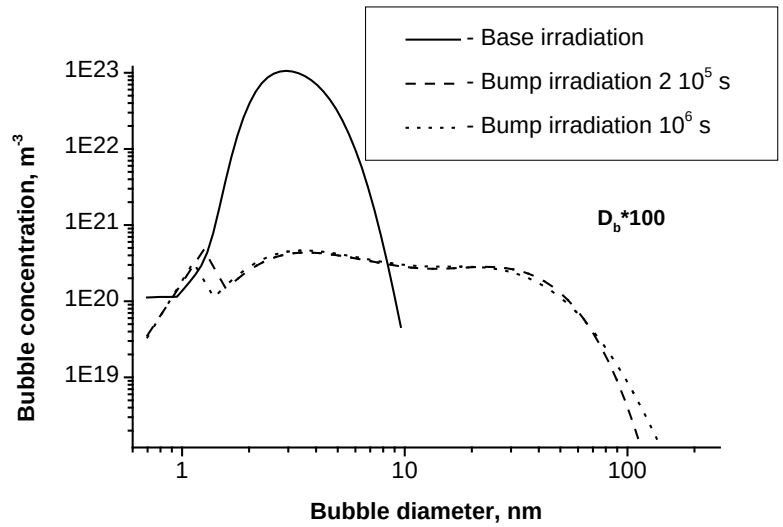

Fig. 3.5. The same as in Fig. 3.4 but with diffusion coefficient of bubbles multiplied by a factor of 100.

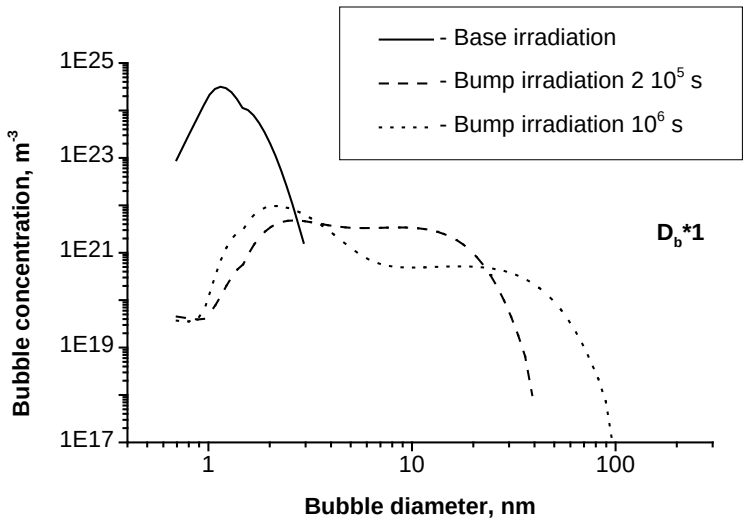

Fig. 3.6. Size distribution function of intragranular bubbles calculated by MFPR with advanced model for gas re-solution from bubbles.

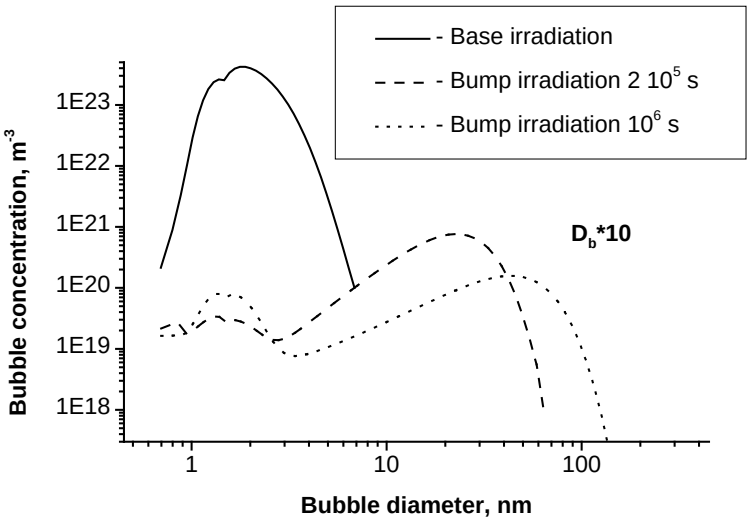

Fig. 3.7. The same as in Fig. 3.6 but with diffusion coefficient of bubbles multiplied by a factor of 10.

4. Irradiation effects on intergranular bubbles

In the majority of the currently existing models for gas release from UO_2 fuel, it is assumed that during steady-state reactor operation the grain boundary bubbles increase in size and number until they touch, allowing gas release to the fuel/clad gap [4, 13–15]. The grain boundary bubbles appear to be relatively immobile, particularly at temperatures below about 1900 K [16], and it is usually assumed that gas release occurs only on interlinking. The time for the "grain-face porosity saturation" to occur corresponds with an incubation time period of bubble growth [13]. It is generally accepted now that the grain face porosity saturates at the fractional coverage of the grain boundaries occupied by bubbles ≈ 50%, and commencement of gas release from grain faces to edges (and further through the edge tunnels outside the grain) is usually associated with the formation of the open porosity network at this coverage [4, 13–15].

However, in recent tests [17, 18] this conclusion on the commencement of gas release was not confirmed. In these tests the 3 and 4 BWR cycle specimens with ≈ 2.4 and 2.9% burnup, respectively, were taken from the outer pellet region (between rim and middle), and the fractional coverage of grain faces by bubbles was evaluated from SEM photographs as ≈ 6 and 10% [18], respectively, see Fig. 4.1. Despite such low values of the grain face coverage, significant fractional fission gas release (up to 21%) during their base irradiation was measured by pin puncture tests from these specimens, Fig. 4.2. Therefore, a noticeable gas release from these fuel samples occurred at a coverage far below the saturation value ≈ 50% and without visible bubble interlinking on the grain faces. The irradiation temperature at the location of the specimens was not directly measured, but might be evaluated to be about ≤ 1000°C from their maximium linear heat generation rates (between 300 and 370 W/cm).

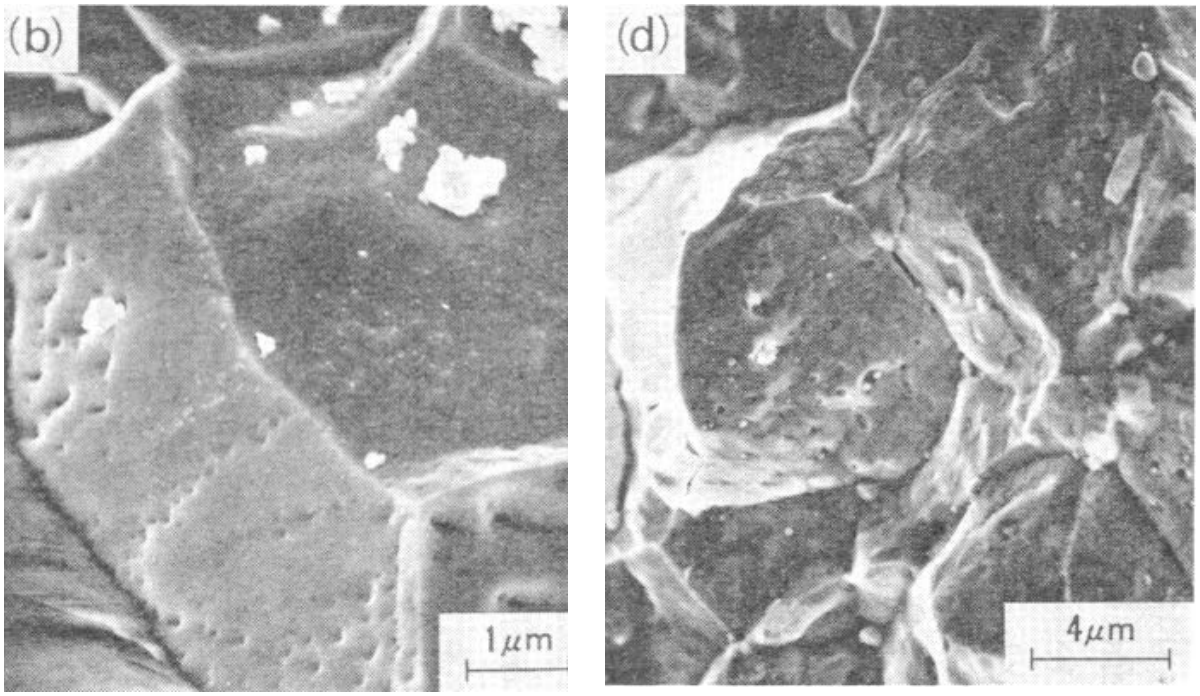

Fig. 4.1. Scanning electron micrographs of fractured surface of as-irradiated specimens (from [17]).

On the other hand, a significant burst release observed in these tests during post-irradiation annealing at 1600–1800°C was invariably associated in [17, 18] with the coverage of about 40–50% attained under various burnups and heating conditions, Fig. 4.3. Hence, interlinking of grain face bubbles at the threshold value of the coverage ≈ 50% considered in the models [4, 13–15] might be responsible for the secondary burst release observed in the annealing stage of the tests [17, 18].

Therefore, from these tests it can be generally concluded that at low irradiation temperatures (≤ 1000°C) the formation of the open porosity network can be significantly delayed, but this does not prevent the commencement of gas release. Indeed, 4 irradiation cycles were insufficient for the attainment of the saturation coverage, whereas gas release was significant (10–20%) at a rather low coverage 6–10%. On the other hand, under normal operation conditions of the water reactors an essential outer part of the fuel pellet is located in the low temperature (< 1000 °C) zone.

To avoid this contradiction, one should additionally consider an input in the total gas release of the diffusion transport of gas atoms along grain faces, which becomes dominant in the lack of interlinking of grain face bubbles. Usually this diffusion process is considered only in evaluation of the grain face bubble size [9, 19–21] and/or estimation of the incubation period for saturation coverage [4, 14], since it is assumed that practically all the gas diffused from grains to grain boundaries is collected by the growing grain face bubbles and only a negligible part is transported to grain edges (before interlinking of grain bubbles). This assumption was seemingly supported by the theoretical paper [21] where it was shown that the sink strength of the grain face periphery (edges) becomes (after some initial time interval) negligibly small in comparison with the total sink strength of the growing grain face bubbles. However, as will be shown below, this conclusion can be strongly violated if one additionally considers re-solution of gas atoms from face bubbles back to the grain matrix (not considered in [21]), that may essentially redistribute the outcoming diffusion flux from grains among different sinks on grain faces. On the other hand, such a process of gas atom re-solution from grain faces was considered in other papers (say, [22, 9, 4]), however, in these papers the grain face diffusion transport to edges was not included in consideration.

In a recent paper [23] an attempt of simultaneous consideration of both these processes (grain face diffusion and re-solution from the grain boundary) was made, however, consideration of the re-solution process was not consistent with calculation of the outcoming flux deposited on the grain boundary. Indeed, as shown in [22] re-dissolved atoms are knocked some distance δ into the grain from the grain boundary, whence they may proceed to diffuse again. The built-up concentration barrier c_δ of the resolution layer reduces the diffusion flux from the grain J_{dif}, on the one hand, and determines the net flux of atoms deposited on the grain boundary $J_\delta = Dc_\delta/\delta$, on the other hand [22]. This flux J_δ should counterbalance the resolution flux back into the grain J_{res} and, in accordance with the flux matches $J_{dif} + J_{res} = J_\delta$ (see below), may essentially exceed the "source term" from the grain J_{dif}. Namely this flux J_δ should be redistributed among various grain face sinks (bubbles and edges) rather than the source term flux J_{dif}. Neglecting such an effect, the author [23] also strongly underestimated the grain boundary diffusion flux to edges (but for other reasons than [21]).

In the present paper a completely self-consistent scheme for consideration of diffusion and re-solution processes in the grain and grain faces is proposed. It will be shown that "circulation" of gas atoms collected by growing intergranular bubbles from the grain face and then returned back (by the resolution process) into the grain matrix, makes bubbles much less effective sinks for gas atoms in the course of their growth saturation (i.e. approaching a balance among absorbed and re-emitted atoms) and thus continuously increases a fraction of the source term flux J_{dif} eventually transported to edges. In particular, this leads to a natural conclusion that in the limiting case of the complete balance and cessation of the face bubble growth (before their interlinking), 100% of the source term flux will be transported to grain edges via grain face diffusion process.

Implementation in the MFPR code of the improved model of the grain face porosity based on consideration of radiation effects on intergranular bubbles, and numerical treatment with the new model of various available data on gas release from irradiated fuel, allow a satisfactory agreement with measurements.

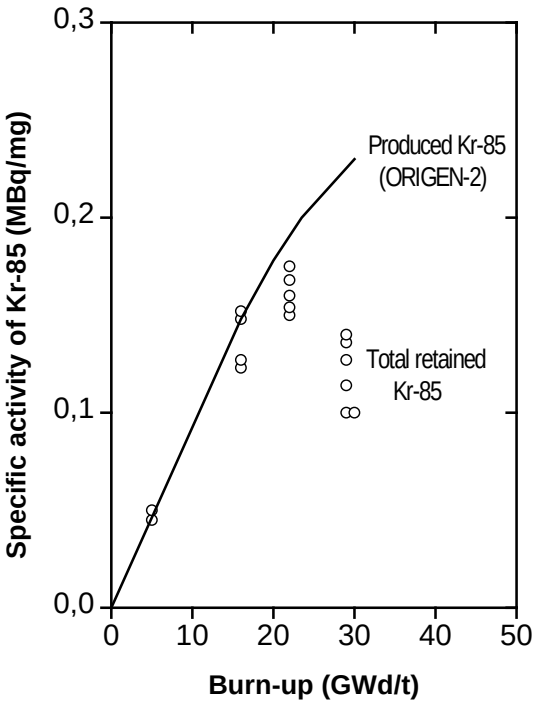

Fig. 4.2. *^{85}Kr concentrations in UO_2 as a function of burn-up (from [17]).*

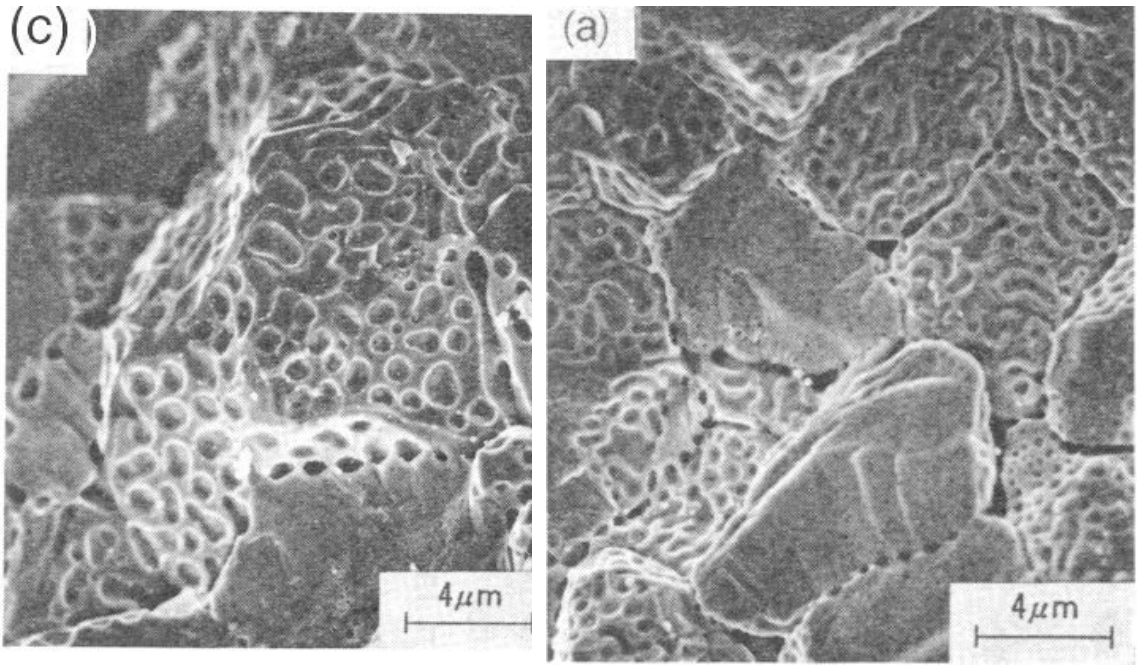

2 cycle specimen 4 cycle specimen

Fig. 4.3. *Scanning electron micrographs of fractured surface of post-irradiated specimens heated up to 1800 °C (from [17]).*

4.1. Model description

Owing to an extremely high ratio of the gas atom diffusion coefficients on grain faces D_f and in the grain matrix D_g, which is usually believed to be of the same order of magnitude as that for the uranium self-diffusion coefficients, $D_f/D_g \sim 10^5$ [24], one can apply results of the steady-state consideration of the grain face diffusion problem [20] to calculate the face bubbles and edges sink strengths in the mean field approximation:

$$(k_e R_f)^2 = 2k_b R_f \mathrm{I}_1(k_b R_f)/\mathrm{I}_2(k_b R_f), \tag{4.1}$$

where k_e^2 and k_b^2 are the total sink strengths of the grain face edges and bubbles; I_1 and I_2 represent the first and the second modified Bessel functions of the first kind, respectively; R_f is the grain face radius. For the Tucker's quasi-spherical "toroid" model of the UO_2 grain [25], each grain has fourteen identical circular faces with radius approximated as $R_f = (2/\sqrt{14})R_g$, where R_g is the grain radius.

The corrected expression for the bubbles sink strength in a cellular model in which each face bubble with a mean radius R_b in the plane of the grain boundary is surrounded by a concentric sink-free region with radius R_s [20], takes the form:

$$(k_b R_s)^2 = 8(1-\varphi)^2/[(1-\varphi)(\varphi-3) - 2\ln\varphi], \tag{4.2}$$

where $\varphi = (R_b/R_s)^2$ is the grain face coverage.

In such a (mean field) approximation, if fission gas is deposited uniformly at some rate $2J_\delta$ atoms per unit area of face on each grain face from two adjacent grains, $2J_\delta\,\varphi$ goes directly to face bubbles. The flow distribution of the remainder between the face bubbles J_b and edges J_e may be described by the following equations:

$$J_b = k_b^2 D_f \tilde{c}\ \pi R_f^2, \tag{4.3}$$

and

$$J_e = k_e^2 D_f \tilde{c}\ \pi R_f^2, \tag{4.4}$$

where $\tilde{c}$ is the mean concentration of gas atoms dissolved in the grain boundary, which can be calculated from the steady-state balance equation:

$$2J_\delta(1-\varphi) = (k_e^2 + k_b^2) D_f \tilde{c}\ . \tag{4.5}$$

As explained above, the deposition rate J_δ cannot be equated to the diffusion source term J_{dif} from the grains, since gas atoms re-emitted from the face bubbles to the grains (in some resolution layer with the thickness δ around the grain face) will tend to return back to the grain face sink, thus increasing the net flux onto the grain face. This flux J_δ has to counterbalance the resolution flux back into the grains J_{res} and thus obeys the flux matches in the vicinity δ of the grain boundary:

$$J_{dif} + J_{res} = J_\delta. \tag{4.6}$$

Therefore, the calculation of the deposited flux also requires evaluation of the resolution flux J_{res} from the grain face.

Usually the resolution flux J_{res} (into each of two adjacent grains) is evaluated as $b_v N_f/2$, where b_v is the resolution probability and N_f is the number of atoms per unit area of the grain face [4, 13–15], i.e. by smearing over the grain face surface structure. For this reason, the resolution flux does not depend on the amount and size of face bubbles but depends only on the total amount of gas atoms in the bubbles. Such a consideration significantly simplifies the resolution process modelling, however, prevents from correct description of the grain face diffusion fluxes redistribution among various surface sinks.

Indeed, since in reality gas atoms are deposited over the whole grain face area (unoccupied and covered by bubbles), but are emitted into the grains only from the face bubbles, some "circulation" of gas atoms (coming from and returning back into the grains) through the grain face bubbles occurs. The emission rate increases with the bubble size growth, thus, for instance, under certain conditions may completely counterbalance the absorption rate, leading to the cessation of the grain face bubbles growth. Under such conditions the absorbed by bubbles part of the deposited flux J_δ will be completely returned back to the grains by the resolution flux J_{res}, therefore, the source term flux J_{dif} will be completely transported to the grain edges. Under more general conditions of continuously growing bubbles (up to their interlinking) the gas atoms absorption will be compensated by the resolution process only partially, thus reducing the flux J_e to the edges. However, in all the cases this flux J_e will be significantly higher than one calculated in neglect of the above described circulation process.

To calculate the resolution flux J_{res}, one should also take into account that according to the Nelson's model [8] for intragranular bubbles, the resolution rate is independent of the bubble size only for very small bubbles ($R_b \leq$ 1–1.5 nm). For larger spherical bubbles only a fraction of gas atoms within a critical distance from the bubble surface $\lambda \approx$ 1 - 1.5 nm may be escaped, therefore, the resolution rate becomes inversely proportional to the bubble radius, $b_0 N_b (\lambda/R_b)$, where b_0 is the resolution probability and N_b is the number of atoms in a bubble. Despite the grain face bubbles have a more complicated form, this conclusion can be generalised also for lenticular bubbles with a radius R_b in the plane of the grain boundary, probably, with some renormalisation of the resolution parameters b_0 and λ. In the following calculations, for simplicity the same values of these parameters as for the spherical bubbles, will be used, i.e. $\lambda \approx$ 1–1.5 nm [8] and $b_0 \approx (2–3)\cdot 10^{-17}$ cm^3 [1].

Substitution of these values in the flux matches, Eq. (4.6) for each of two adjacent grains, results in:

$$J_\delta = J_{dif} + b\, N_b /2\pi R_s^2, \tag{4.7}$$

where $b \approx b_0\lambda/(\lambda + R_b)$.

This equation determines the mean gas atom concentration $\tilde{c}$ in the grain face by its substitution in the balance Eq. (4.5):

$$2\,(J_{dif} + bN_b /2\pi R_s^2)\,(1 - \varphi) = (k_e^2 + k_b^2) D_f \tilde{c}\ . \tag{4.8}$$

The source term flux J_{dif} entering in Eq. (4.8), should be self-consistently calculated with the new boundary condition $c = c_\delta$ at the resolution layer boundary δ, as recommended by Turnbull [9].

The competition between the absorption and resolution processes determines the growth rate of a bubble:

$$\mathrm{d}N_b/\mathrm{d}t = k_b^2 \pi R_s^2 D_f\ \tilde{c} + 2J_\delta \pi R_b^2 - bN_b\,. \tag{4.9}$$

The volume of a grain face lenticular bubble is

$$V_b = (4\pi/3) R_b^3 f(\theta), \tag{4.10}$$

where $f(\theta) = 1 - (3/2)\cos\theta + (1/2)\cos^3\theta$, and the accepted value for UO_2 is 50° (e.g. [4]).

Under assumption that the pressure P inside the bubble balances the capillary forces restraining the bubble in addition to any external pressure P_{ext}, and using the ideal gas law (valid for relatively large grain face bubbles with $R_b >$ 5 nm), one gets

$$N_b = PV_b/kT = (4\pi R_b^3/3kT)\, f(\theta)(P_{ext} + 2\gamma/R_b), \tag{4.11}$$

where γ is the free surface energy (e.g. [4]).

The radius R_s of a concentric sink-free region around each bubble is determined by the mean number density c_b of bubbles on a grain face $R_s \approx (\pi c_b)^{-1/2}$, which was visually analysed in several independent tests, e.g. [18, 26, 27]. In all these observations the bubble number density varied in the range $c_b \approx 10^{11}$–10^{13} m^{-2} and might be fairly well approximated by the formula:

$$c_b = 3.67\cdot 10^8 \cdot \exp(1.314\cdot 10^4/T)\ \mathrm{m}^{-2}, \tag{4.12}$$

[T] = K in a wide temperature interval 800–1900°C. At low temperatures the concentration was limited by the value of 10^{13} m^{-2}.

4.2. Model implementation in MFPR code

According to the present model, the number of bubbles on a grain face N_{bpf} is a function of grain size and temperature:

$$N_{bpf} = \left(R_f / R_s\right)^2 = 4\pi c_b R_g^2 / N_f \ ,$$

where N_f = 14 is the number of faces per grain.

Evolution of the average number of atoms comprising a face bubble is determined by Eq. (4.9), which after substitution of Eqs. (4.7) and (4.8) takes form:

$$\frac{dN_b}{dt} = 2\pi \frac{k_b^2 R_s^2 + k_e^2 R_b^2}{k_b^2 + k_e^2} J_{dif} - \frac{k_e^2}{k_b^2 + k_e^2}\left(1 - \left(\frac{R_b}{R_s}\right)^2\right) b N_b \,, \tag{4.13}$$

where $b = b_0\lambda/(\lambda + R_b)$ is the irradiation-induced re-solution rate from bubbles.

In the MFPR code the source term flux J_{dif} is calculated as a result of overall release of atoms out of a grain due to different processes (diffusion and biased migration of gas atoms and bubbles, grain boundary sweeping).

Total number of gas atoms comprising grain face bubbles Y_f is related to the average number of atoms per a face bubble by an obvious formula:

$$Y_f = N_b N_{bpf} N_f N_{gr}/2, \tag{4.14}$$

where N_{gr} is the number of grains in the considered fuel sample.

The model implemented in the code for the description of edge bubbles is presented in [2]. According to the MFPR model, the rate of gain of gas atoms comprising grain edge bubbles Y_e can be represented in the form:

$$\frac{dY_e}{dt} = J_{dif}\, 4\pi R_g^2 N_{gr} - \frac{dY_f}{dt} \tag{4.15}$$

Interconnected edge tunnels are formed at the critical grain edge swelling $B^0_{vcrit} \approx 5\%$, and determine the onset of gas release from the grain.

Thus, at each time step determined by the evolution of the intergranular system, Eq. (4.13) is numerically solved by the fourth-order Runge-Kutta scheme with adaptive time step, then values of Y_f and Y_e are found from Eqs. (4.14) and (4.15).

Average number of atoms comprising a face bubble is governed by Eq. (4.13) up to the moment of interlinkage of face bubbles, which is assumed to take place at the critical coverage $A^* \approx 50\%$. There upon the growth of face bubbles ceases and a standard approach to the problem of fission products release through the grain face open porosity is applied.

4.3. Model validation

There are several experimental works where microscopic behaviour of intergranular bubbles was observed directly [17, 26]. As mentioned before, in [17] the specimens were taken from UO_2 pellets irradiated in commercial BWR (burn-up: 6~28 GWd/t) at a point between the fuel rim and middle. Grain face bubble concentration and fractional coverage were examined by scanning electron microscope fractography. In addition, radii of face bubbles were also evaluated (see Figs. 4.1 and 4.3). The irradiation temperature at the location of the specimens may be roughly evaluated to be about ≤ 1000°C from their maximum linear heat generation rates

(between 300 and 370 W/cm). The grain sizes of the fuel and irradiation rate were approximately equal to 9 μm and $1.8 \cdot 10^{19}$ $m^{-3}s^{-1}$, correspondingly. During irradiation the concentration of the intergranular bubbles increased from $\sim 1.6 \cdot 10^{13}$ m^{-2} (at burn-up ~16 GWtd/t) to $\sim 4 \cdot 10^{13}$ m^{-2} (at burn-up $\sim$ 23 GWtd/t) and then dropped to $\sim 1.6 \cdot 10^{12}$ m^{-2} (at burn-up $\sim$ 28 GWtd/t). Such a temporal behaviour of the bubble concentration well correlates with the assumption of [27] that the grain face bubble coarsening occurs at a late stage of irradiation leading to the reduction of the bubble concentration, however, is not considered in the current model. For this reason, in the current calculations the concentration of face bubbles was fixed at the terminal value $1.6 \cdot 10^{12}$ m^{-2} measured in [17, 18], being in a good agreement with the prediction of Eq. (4.12) at 1000°C. Correspondingly, results of the model calculations are compared with the terminal values measured in [17, 18] in Table 4.1.

Table 4.1. Modelling of experiments [17, 18]

	Face bubble diameter, nm	Fractional coverage, %	Kr release, %
MFPR calculations	216	5.9	10
Experiment	229	10.1	20

It should be noted that all the data [17, 18] are quite widely scattered from grain to grain and the measured values may be considered only as estimations. For instance, fractional coverage obtained in [18] by image analysis (see Table 4.1, column 3) is almost two times larger than ones calculated from the measured bubble mean size and concentration: $\pi R_b^2 c_b \cdot 100\% \approx 6.6\%$, that is in a much better agreement with the model calculation $\approx 5.9\%$. A rather strong uncertainty in the gas release data can be clearly seen from Fig. 4.2.

In the other experiment [26] UO_2 fuel irradiated to a burn-up of $2 \cdot 10^{26}$ m^{-3} with fission rate $\approx 2.6 \cdot 10^{19}$ $s^{-1}m^{-3}$ was examined by transmission and scanning electron microscopy and replication metallography. In these tests gas release was not measured, however, the fission gas distribution on the grain boundaries was characterised as a function of irradiation temperature 750–1350°C.

Results of the experiments [26] modelling with the basic set of the MFPR internal parameters are presented in Table 4.2 containing the calculated and measured values of radii and concentrations of face bubbles.

Table 4.2. Modelling of experiments [26]

	Face bubble radius, μm			Face bubble concentration, m^{-2}		
	T=1023 K	T=1423 K	T=1623 K	T=1023 K	T= 1423 K	T=1623 K
MFPR calculations Chemistry off	0.020	0.1	0.36	$1.0 \cdot 10^{13}$	$3.7 \cdot 10^{12}$	$1.2 \cdot 10^{12}$
MFPR calculations Chemistry on	0.021	0.2	0.36	–	–	–
Experiment	0.03	0.3–0.5	0.5	$7.5 \cdot 10^{12}$	$1.2 \cdot 10^{12}$	$2.0 \cdot 10^{12}$

As seen from Table 4.2, results of bubble radius calculation can be slightly improved by additional consideration of fission products other than Xe and Kr ("chemistry on"). Taking into account a wide scattering of the experimental data, the agreement between experimental and calculation results can be considered as quite satisfactory.

After validation of the new model for the grain face bubble evolution against microscopic observations of the grain face structure in [17, 26], the MFPR module with the newly implemented model was additionally verified against the integral data for gas release and fuel swelling in the Zimmermann's tests [28].

The results of calculations with the MFPR code for conditions of the Zimmermann's experiments are presented in Fig. 4.4. In the tests [28] of the steady-state type, the fission gas release has been evaluated by comparison of the measured concentration of the retained fission gas and actual values of the generated gas. As one can see from Fig. 4.4, application of the improved model of gas transport along grain faces provides about 30% earlier beginning of fission gas release from UO_2 fuel as compared with the old MFPR version.

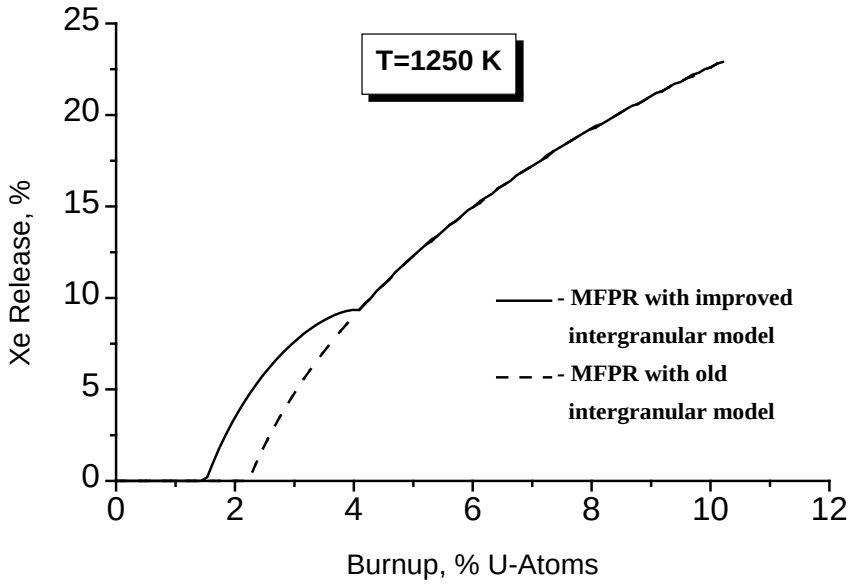

Fig. 4.4. Xe release from UO_2 as a function of burn-up for conditions of Zimmermann's tests [28] at T = 1250 K, calculated by two versions of the MFPR code.

Commencement of fission gas release at temperature 1250 K in [28] occurred at burn-up < 2%, that is in a good agreement with the calculated burn-up value 1.5%. As temperature increases, the difference between the two MFPR versions calculations decreases. For example, at temperature 1500 K the onset of Xe release occurs at 0.7 % burn-up in the new version and at 0.9 % burn-up in the old one. At this temperature the data presented in [28] allows an accurate determination of the fission gas release commencement at 0.6 % burn-up, which well corresponds to the calculation results with the new MFPR version. At lower temperatures T < 1000°C the difference in the prediction of the gas release onset by the two versions of the MFPR code increases (Fig. 4.5), this determines qualitatively different behaviour of gas release from the extended outer zone of real fuel pellets.

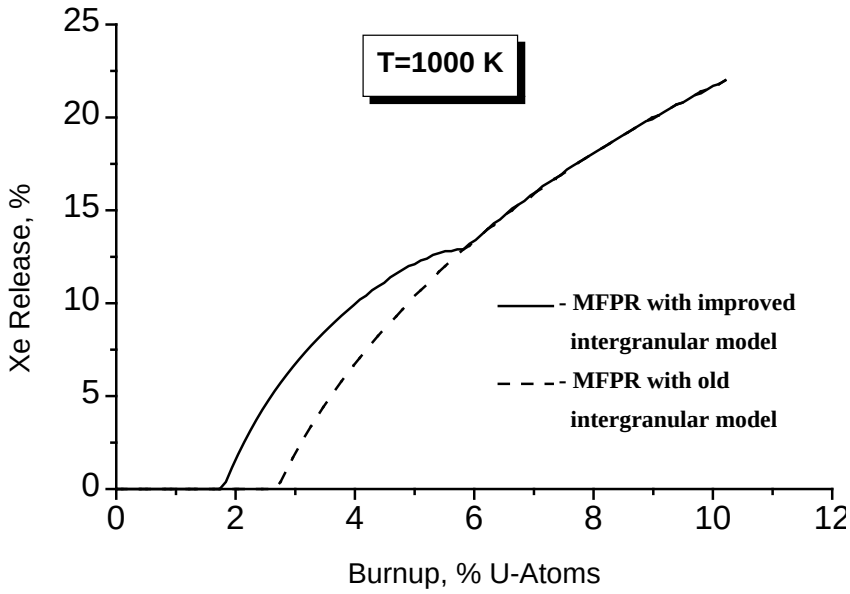

Fig. 4.5. *The same as in Fig. 4.4 but for T = 1000 K.*

Besides timing of gas release, the implemented model of intergranular transport also controls fuel swelling due to grain face porosity. The predictions of total fuel swelling obtained by the old and new MFPR versions are shown in Figs. 4.6 and 4.7. In the previous version of MFPR ten bubbles per grain face was fixed at all temperatures. Owing to such an assumption, the intergranular swelling saturated at the level of ~10% independently on temperature (see Fig. 4.6), in an apparent contradiction with the experimental observations [28]. Implementation into MFPR of the improved model of the grain face porosity based on consideration of radiation effects on intergranular bubbles, allows more adequate simulation of the fuel swelling, Fig. 4.7.

4.4. Conclusions

A new advanced model for the irradiation effects on grain face bubbles based on the self-consistent consideration of diffusion and re-solution processes in the grain and grain faces, is developed. An important role of grain boundary diffusion of gas atoms to edges before interlinking of intergranular bubbles, is outlined.

Implementation in the MFPR code of the new model and numerical treatment of various available data on gas release from irradiated fuel, show a satisfactory agreement of the code predictions with measurements. Calculations of the intergranular bubbles growth kinetics are also in a fair agreement with the grain face microstructure observations.

As a result, an important conclusion is derived that at low irradiation temperatures ($\leq 1000^{\circ}$C) gas release commences significantly earlier than predicted by the previous code version and, for this reason, the total gas release during an extended irradiation period (up to 6 at.% burn-up) noticeably increases. This leads to important consequences with respect to the gas release predictions for the real fuel pellets, since under normal operation conditions of the water reactors a significant outer part of the fuel pellet is located in the low temperature ($< 1000\ ^{\circ}$C) zone.

An additional validation of the new code version against the fuel swelling measurements allows a significant improvement in the code predictions also in this area..

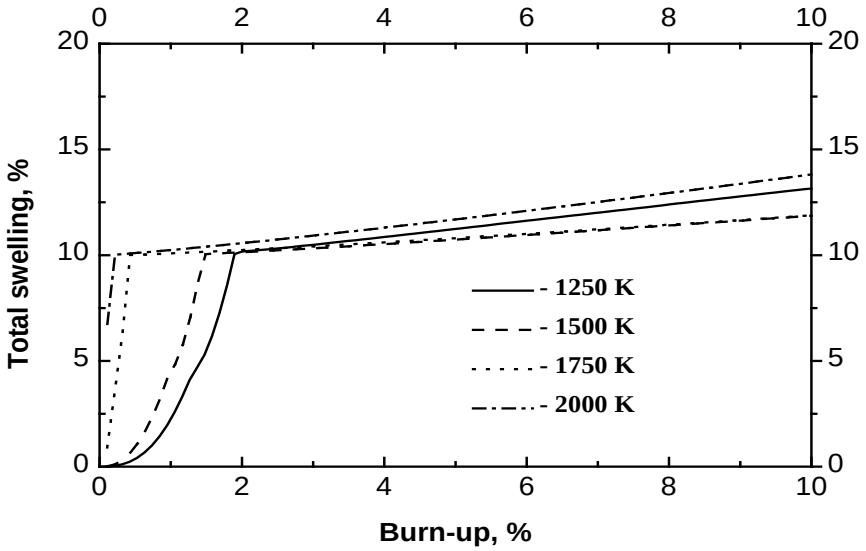

Fig. 4.6. *Unrestrained swelling for conditions of Zimmermann's tests [28] calculated by the previous MFPR version.*

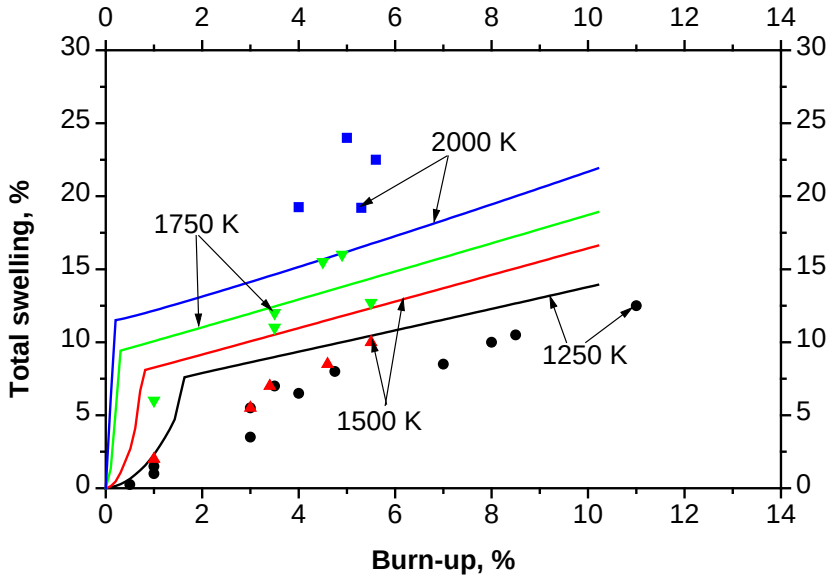

Fig. 4.7. *Swelling calculated by the new MFPR version with account for contribution of solid fission products into total swelling. Data points are from [28].*

5. Thermal re-solution effects

As demonstrated in [1], at high temperatures the thermal re-solution effects determine the mechanism of bubble nucleation and may influence the gas system behaviour during high temperature annealing of irradiated fuel. The standard kinetic equation for the number N_b of gas atoms in a bubble with the radius R_b under irradiation conditions:

$$dN_b/dt = 4\pi D_g c_g R_b[1 - K_g N_b/(4\pi D_g c_g R_b)], \quad (5.1)$$

with the account for the thermal re-solution of gas atoms from a bubble in the Van-der-Waals approximation, transforms into the following one:

$$dN_b/dt = 4\pi D_g c_g R_b[1 - K_g N_b/(4\pi D_g c_g R_b) - (P/P_e) \exp(B_{Xe} (P - P_e)/kT)], \quad (5.2)$$

where D_g and c_g are the gas atom diffusion coefficient and bulk concentration (number of gas atoms per U atom), respectively; K_g is the radiation induced re-solution rate, $P = kTN_b/(4\pi R_b^3/3 - B_{Xe}N)$ is the bubble pressure ($P >> P_h$, where P_h - external pressure), $B_{Xe} \approx 8.5 \cdot 10^{-29}$ m^3/atom is the Van-der-Waals constant for Xe gas, and P_e is the partial gas pressure in equilibrium with the solid solution of gas atoms with concentration c_g in the fuel matrix.

Assuming Henry's law behaviour up to the terminal solubility, one gets $P_e = K_s^{-1} c_g$ with the constant value K_s. This assumption allows simplification of the system behaviour analysis which was performed in [1] and demonstrated that at high temperatures the thermal re-solution process determines the onset of bubble nucleation under steady irradiation conditions, and significantly influences the gas system behaviour during high temperature annealing of irradiated fuel.

However, as shown below, application of a more realistic solubility law that accounts for corrections to the thermodynamic state of gas atoms in equilibrium with a high pressure gas (that obeys a non-ideal equation of state), leads to a noticeable suppression of the thermal resolution effects (especially in the annealing stage), nonetheless, still determines bubble nucleation process under irradiation at high temperatures.

5.1. Model for thermal re-solution of gas atoms from bubbles (Van-der-Waals approximation)

In the completely self-consistent scheme Henry's law is modified by consideration of the thermodynamic equilibrium between the gas phase at a given high pressure P and gas atoms in the ideal (diluted) solid solution:

$$c_g = P_e K_s \varphi(P,T), \quad (5.3)$$

where

$$\varphi(P,T) = \exp(B_{Xe}P/kT), \quad (5.4)$$

is the function accounting for the gas phase non-ideality (typical for small bubbles with $R_b \leq 5$ nm) in the Van-der-Waals approximation, so that $\varphi(P,T) \to 1$ as the gas phase approaches to the ideal state.

Correspondingly, Eq. (5.2) takes the form:

$$dN_b/dt = 4\pi D_g c_g R_b[1 - K_g N_b/(4\pi D_g c_g R_b) - c_g^{eq}/c_g], \quad (5.5)$$

where

$$c_g^{eq} = P K_s \varphi(P,T). \quad (5.6)$$

The temperature dependence of K_s is supposed to be of Arrhenius type:

$$K_S(T) = K_S(T_0)\exp\left(\frac{E_S}{kT_0} - \frac{E_S}{kT}\right), \tag{5.7}$$

where $K_S(T_0)$ is the solubility at a fixed temperature T_0 and E_S is the activation energy of the solid solution.

As seen from Eq. (5.5), both irradiation-induced and thermal re-solution processes (the second and third terms) compete with the capture of gas atoms by bubbles (the first term). The essential difference between the two re-solution mechanisms is their dependence on bubble size. Irradiation-induced re-solution increases with the increase of bubble size, thus it governs the evolution of large bubbles. In contrast, thermal re-solution is shown below to be a fast (exponentially) decreasing function of the bubble size, therefore the effect is most prominent for small bubbles. In particular, it may strongly affect the bubble formation process, especially at high temperatures, due to increase of the gas solubility in the fuel matrix and decrease of the mean steady-state value of gas concentration c_g (that is roughly proportional to D_g^{-1} [1]).

This conclusion is in a qualitative agreement with the steady-irradiation (with fission rate $F \approx 0.9\cdot10^{19}$ m^{-3}s^{-1}, burn-up $\approx 2\cdot10^{26}$ m^{-3}) tests of Baker [29], who observed a complete suppression of the nucleation process at temperatures above 1800–2000°C. In the absence of any noticeable grain growth (and corresponding sweeping of bubbles by grain boundaries) in these tests, the observations can be naturally explained by the thermal re-solution effect that becomes strong for small bubbles at high temperatures (as explained above).

On this basis, quantitative estimations of the thermal re-solution term in Eq. (5.5) and its influence on the bubble nucleation process allow evaluation of $K_s(T_0)$ at temperature $T_0 \approx 2300$ K corresponding to the upper limit of the above presented temperature interval.

Indeed, the condition of the bubble nucleation suppression can be estimated from Eq. (5.5) as

$$c_g^{eq} \geq c_g ,$$

where c_g^{eq} corresponds to the bubble nucleus, i.e. the minimal bubble with the radius $R_{nuc} \approx (3\Omega/\pi)^{1/3}$ (where Ω is the uranium vacancy volume) formed by sticking of two atoms (see [1]).

If one formally extrapolates the standard expression for the equilibrium bubble internal pressure to the small bubble nucleus: $P = 2\gamma / R_{nuc}$, where $\gamma = \gamma_0 - \gamma_1 T$ is the surface tension coefficient with the parameters $\gamma_0 = 1.601376$ J/m^2, and $\gamma_1 = 3.45\cdot10^{-4}$ Jm^{-2}K^{-1}, then Eq. (5.4) can be rewritten in the form:

$$\varphi = \exp\left\{\frac{E^*}{kT} - f_1\right\},$$

where $E^* = 2\gamma_0 B_{Xe} / R_{nuc} \approx 4.85$ eV and $f_1 = 2\gamma_1 B_{Xe} / kR_{nuc} \approx 12.1$. Using Tunbull's evaluation of the gas diffusion coefficient [30]: $D_g \approx D_{g0}^{rad} F + D_{g0}\exp(-E_g / kT)$, where $D_{g0}^{rad} = 3.5\cdot10^{-40}$ m^{2}s^{-1}, $D_{g0} = 7.6\cdot10^{-10}$ m^{2}s^{-1}, $E_g = 3.04$ eV, and the above mentioned evaluation of c_g from [1]:

$$c_g D_g \approx (2\text{–}5)\cdot10^{-23} \text{ m}^2/\text{s},$$

one can finally estimate the solubility as follows:

$$K_s(T_0) \approx 2\cdot10^7 \text{ J}^{-1}. \tag{5.8}$$

The activation energy of the solid solution at high temperatures is evaluated as E_s = 3 eV, in accordance with recommendation of Catlow (see reference [18] in [31]).

5.2. Thermal re-solution from bubbles in the hard spheres approximation

As an alternative, the variant of the thermal re-solution model in the hard spheres approximation for the gas phase [32] in a bubble is considered. In this case the equation of state is written as:

$$P = P_{Xe} F(y)\,, \tag{5.9}$$

where

$$\begin{aligned} &y = \frac{N V_{Xe}}{V},\ V_{Xe} = \frac{4\pi}{3} R_{Xe}^3,\quad P_{Xe} = \frac{kT}{V_{Xe}},\quad R_{Xe} = R_1 - R_2 \ln\left(T / T^*\right), \\ &F(y) = y(1 + y + y^2 - y^3)/(1-y)^3, \end{aligned} \tag{5.10}$$

with the numerical parameters $R_1 = 0.19006$ nm, $R_1 = 0.00889$ nm, $T^* = 231.2$ K.

Consideration of the bubble growth kinetics similar to that in [33, 34] for the Van-der-Waals case, shows that the kinetic equation for the gas bubble has the same form as Eq. (5.5), however, the 'non-ideality' correction φ is given by a more complicated function:

$$\varphi(y) = \frac{y}{F(y)} \exp\left(\frac{3-y}{(1-y)^3} - 3 \right), \tag{5.11}$$

and $\varphi(y) \underset{y\to 0}{\to} 1$.

It is important to note that consideration of the thermal re-solution in the hard spheres approximation, Eq. (5.9) was attempted also in [31, 35-36]. However, mistakes in the final equation similar to Eq. (5.11) (e.g. an additional term $(2\gamma/R_b - P)\Omega/kT$ in the exponential) leads to a significant overestimation of the thermal effect and erroneous predictions for transient and post-irradiation annealing regimes. Indeed, the simplest way to prove that Eq. (5.11) does not have an additional term in exponential is to compare the results for the thermal resolution in the limit $y \to 0$ where Eq. (5.11) should be transformed in the well known expression for the ideal gas law $\varphi(y) \underset{y\to 0}{\to} 1$, as indicated above, independently of the value of $(2\gamma/R_b - P)\Omega/kT$.

The activation energy in the new model was set equal to 3 eV. The solubility was found by the procedure similar to that used above for Van-der-Waals equation of state:

$$K_s(2300\,\mathrm{K}) = 5.3 \cdot 10^{10}\ \mathrm{J}^{-1}. \tag{5.12}$$

Note that this value is three orders of magnitude larger than that calculated for the Van-der-Waals gas, Eq. (5.8). This makes the thermal re-solution dependence on bubble size slower in comparison with the previous (Van-der-Waals) case, however, it is much faster than in the case of the linear Henry's law (either in the approximation of the ideal gas law for bubbles [38], or Van-der-Waals law [1]), i.e. it is still significant only for very small bubbles with a few atoms. For this reason, the main thermal effect relates to the suppression of the bubble nucleation at high temperatures, similar to the Van-der-Waals case, but is insignificant for thermal coarsening during annealing or transient regime. In this sense results of model calculations in both approximations (hard spheres and Van-der-Waals) are qualitatively similar, and for this reason, only results for the Van-der-Waals case will be presented in the following section.

5.3. Model simulations

In order to check the model predictions on the important role of thermal re-solution of gas atoms from bubbles at high temperatures, the MFPR re-solution model was modified by implementation of the thermal re-solution term in the basic kinetic equations for gas atoms and intragranular bubbles. The new code version was validated against several steady-state irradiation and post-irradiation annealing tests.

Dynamics of bubble formation is illustrated in Fig. 5.1 by example of multi-modal simulation of Baker's test [29] in vicinity of the upper critical temperature $T_0 = 2300$ K. In these calculations the temperature was set to constant during irradiation period with the fission rate of 10^{19} $m^{-3}s^{-1}$. As seen, the thermal re-solution effect changes significantly the temporal dependence of the main gas-bubble variables, mean bubble radius, $<R_b>$ and atom-in-bubble concentration, Y_b. In particular, significant delay and sharpening of bubble formation process takes place. This effect is inherent for a wide temperature interval. For example, the time-dependence of bubble characteristics calculated for the same irradiation conditions at low temperatures is illustrated in Fig. 5.2.

As seen from Fig. 5.2, the "incubation" period for bubble nucleation noticeably increases at low temperatures, mainly owing to the athermal character of the gas diffusion coefficient in this temperature range. This allows a self-consistent (with the high-temperature limit) explanation of a significant delay or even complete suppression of bubble nucleation, revealed at temperatures below 800°C in the short-term ($t \le 3 \cdot 10^7$ s) irradiation tests (e.g. [37]).

The effect of partial (at low temperatures) or complete (at high temperatures) suppression of bubble nucleation has a strong influence on intragranular fuel swelling and gas release under steady irradiation conditions, since the capture of gas atoms by bubbles becomes less efficient and thus the diffusion flux to grain faces increases. The model predicts decrease of the critical temperature T_0 for bubble nucleation suppression with decrease of the fission rate, and a strong increase of gas release at high temperatures above T_0 in comparison with the previous MFPR version (without thermal re-solution model), Fig. 5.3. At high fission rate ($F \approx 5 \cdot 10^{19}$ $m^{-3}s^{-1}$) a noticeable increase of gas release is predicted also at low temperatures, Fig. 5.4, whereas the upper critical temperature is shifted to ≈ 2800 K (not shown).

As above mentioned, the thermal effect in the post-irradiation annealing stage is not so significant as it was in the previous model [1]. The new model simulations of the bubble system behaviour during annealing at high temperature 2500 K, Fig. 5.5, show that the thermal coarsening effect still exists, however, the bubble coalescence due to bubble migration prevails. Nevertheless, one should keep in mind that in accordance with Baker's observations [10] the bubble diffusivity might be much smaller than usually proposed (e.g., in the current version of the MFPR code), and in this case the thermal effect becomes more important.

Both these mechanisms of bubble coalescence, however, are not enough strong to explain high gas release and fuel swelling observed during post-irradiation annealing in different tests. Additional mechanisms for intensification of these processes will be studied in the following Section 6.

5.4. Conclusions

The new model for thermal re-solution of gas atoms from bubbles at high temperatures based on the self-consistent consideration of non-ideal gas corrections to the gas state law (in the Van-der-Waals or hard spheres approximation) in small bubbles and to the solubility of gas atoms in the solid matrix in equilibrium with the gas phase at a given pressure (Henry's law), was developed and implemented in the MFPR code.

Results of the modified code validation confirmed that at high temperatures the thermal re-solution process determines the onset of bubble formation under steady irradiation conditions. Namely, the new model predicts a complete suppression of the bubble nucleation process at $T > 2000$°C, in a qualitative agreement with observations of Baker [29], and a significant delay in the onset of the bubble formation at low temperatures $T < 800$°C, as observed in tests [37].

Under conditions of post-irradiation annealing the model predicts the thermal coarsening effect which, however, is not so significant as expected from the previous model [1]. This requires additional mechanisms for modelling of the observed annealing phenomena (see Section 6).

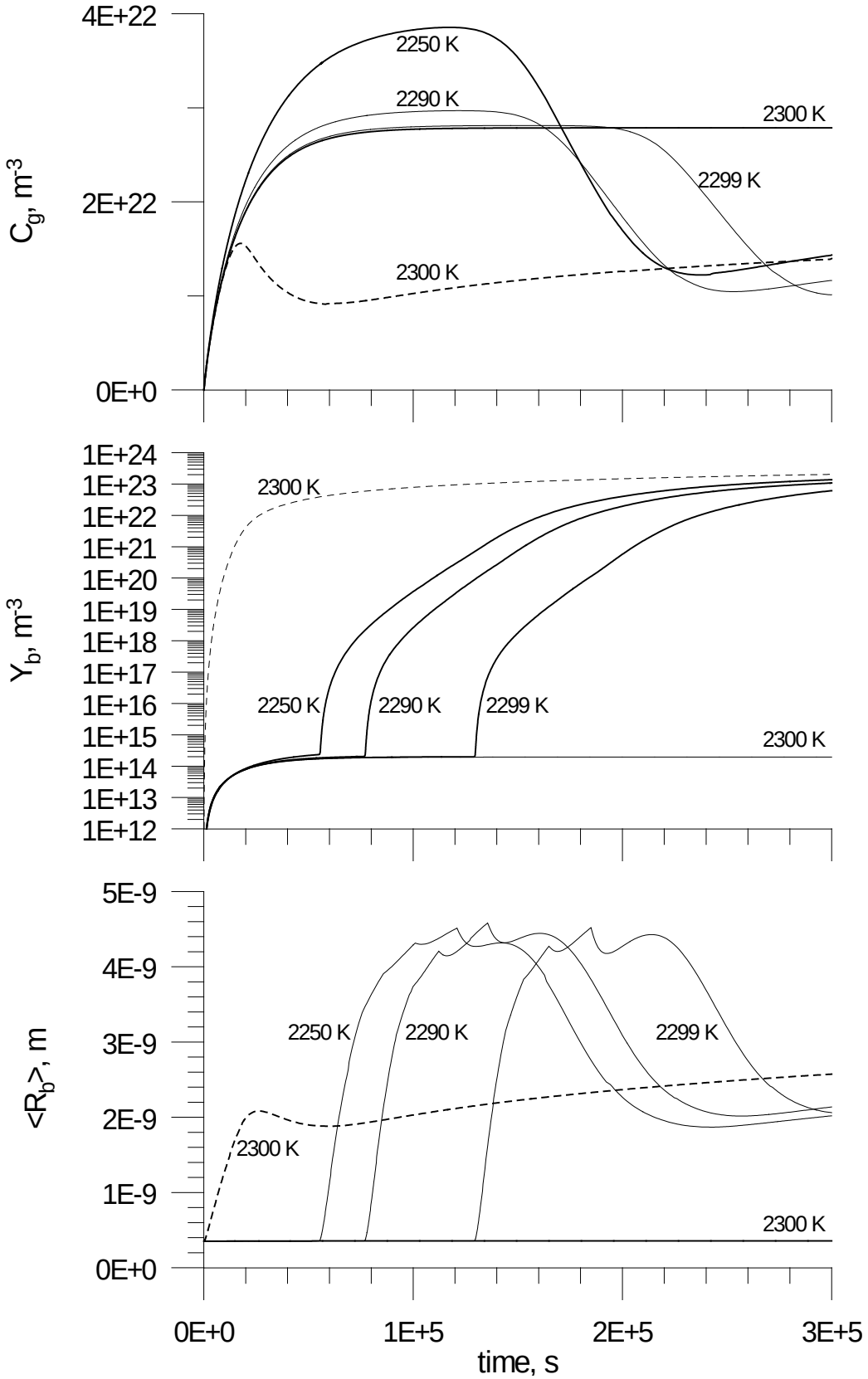

Fig. 5.1. Dynamics of bubble formation process in multi-modal Baker's test simulation. Solid (dashed) lines relate to thermal re-solution option 'on' ('off').

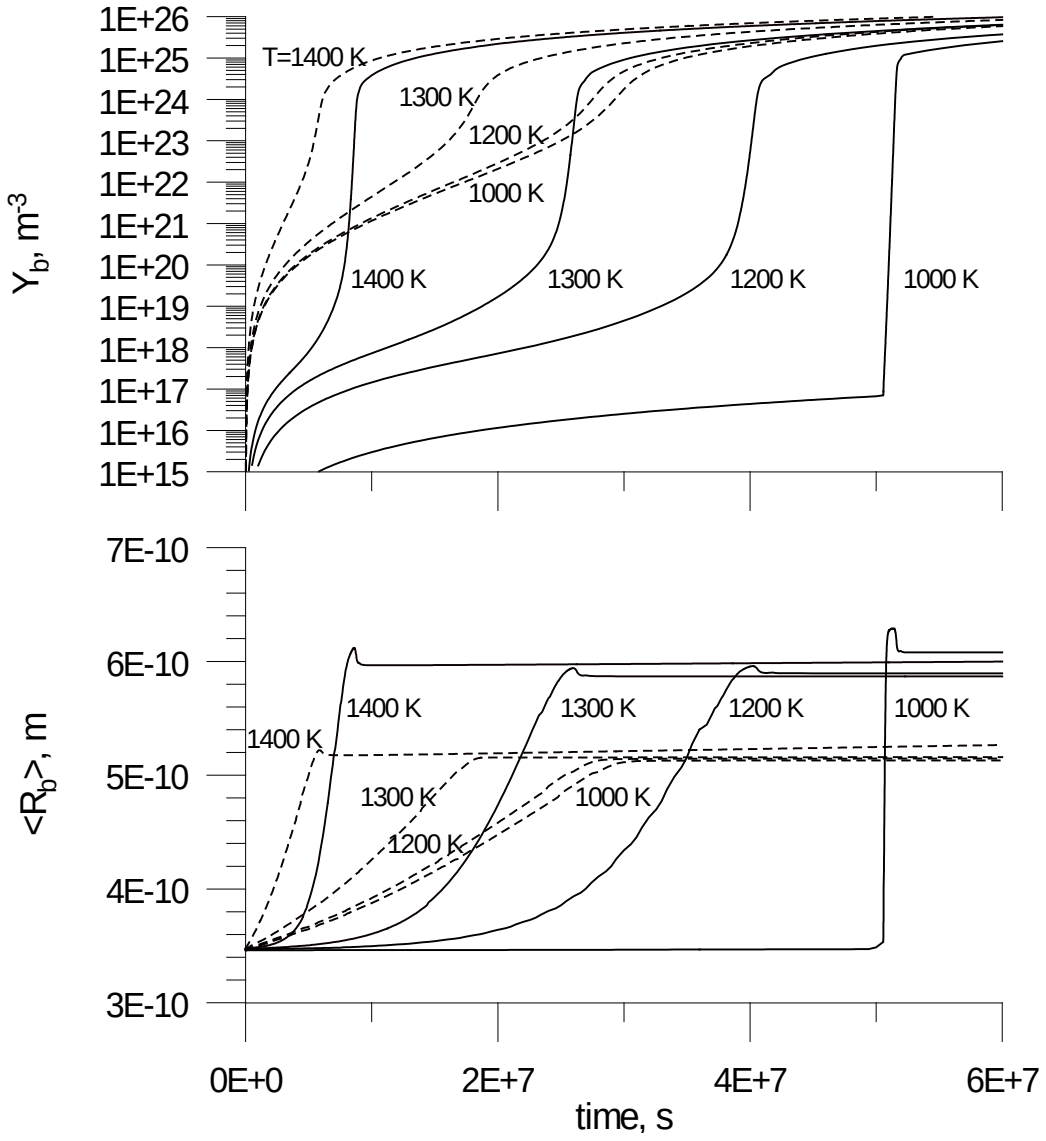

Fig. 5.2. *Evolution of bubble characteristics at low temperatures.*
Solid (dashed) lines relate to thermal re-solution option 'on' ('off').

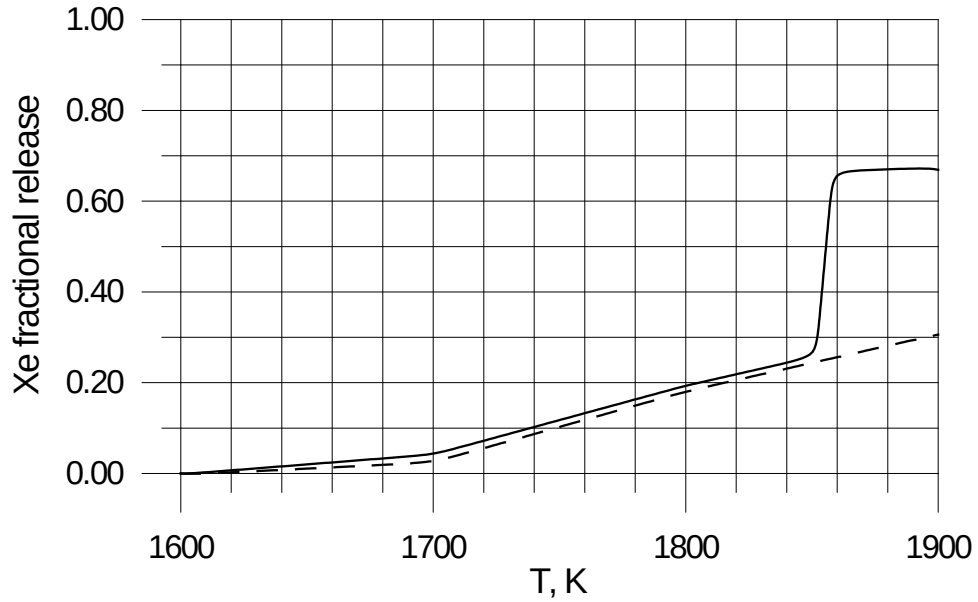

Fig. 5.3. *Thermal re-solution effect under steady irradiation with low fission rate, $F = 10^{18}\ m^{-3}s^{-1}$.*

Model test ($t = 10^{8}$ s, , burn-up = 0.4%). Solid (dashed) lines — thermal re-solution switched on (off).

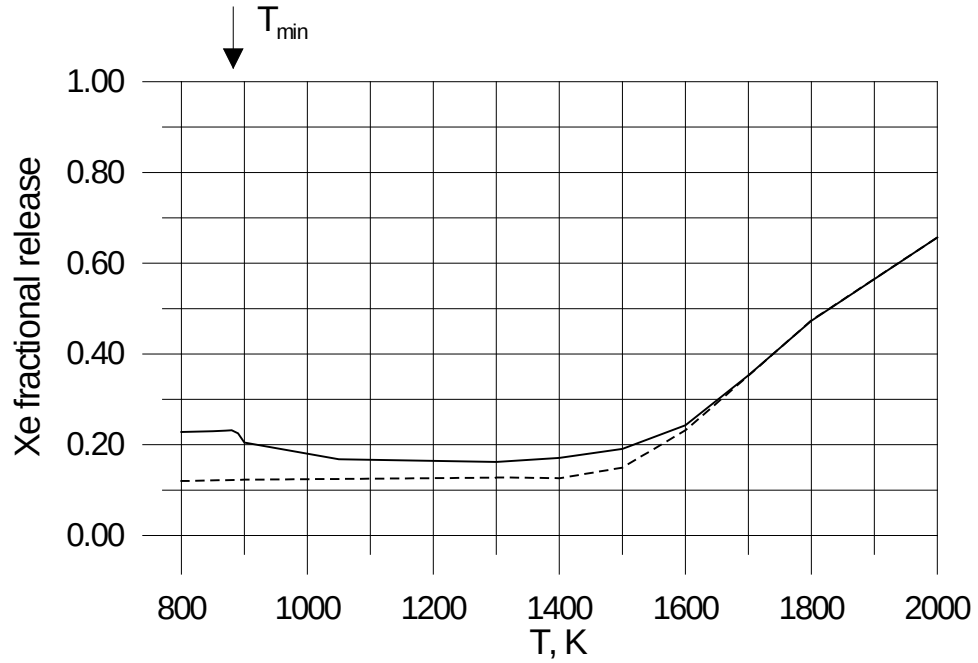

Fig. 5.4. *Thermal re-solution effect under steady irradiation with high fission rate, $F = 5 \cdot 10^{19}\ m^{-3}s^{-1}$.*

Model test ($t = 5 \cdot 10^{7}$ s, burn-up = 10.2%). Solid (dashed) lines — thermal re-solution switched on (off).

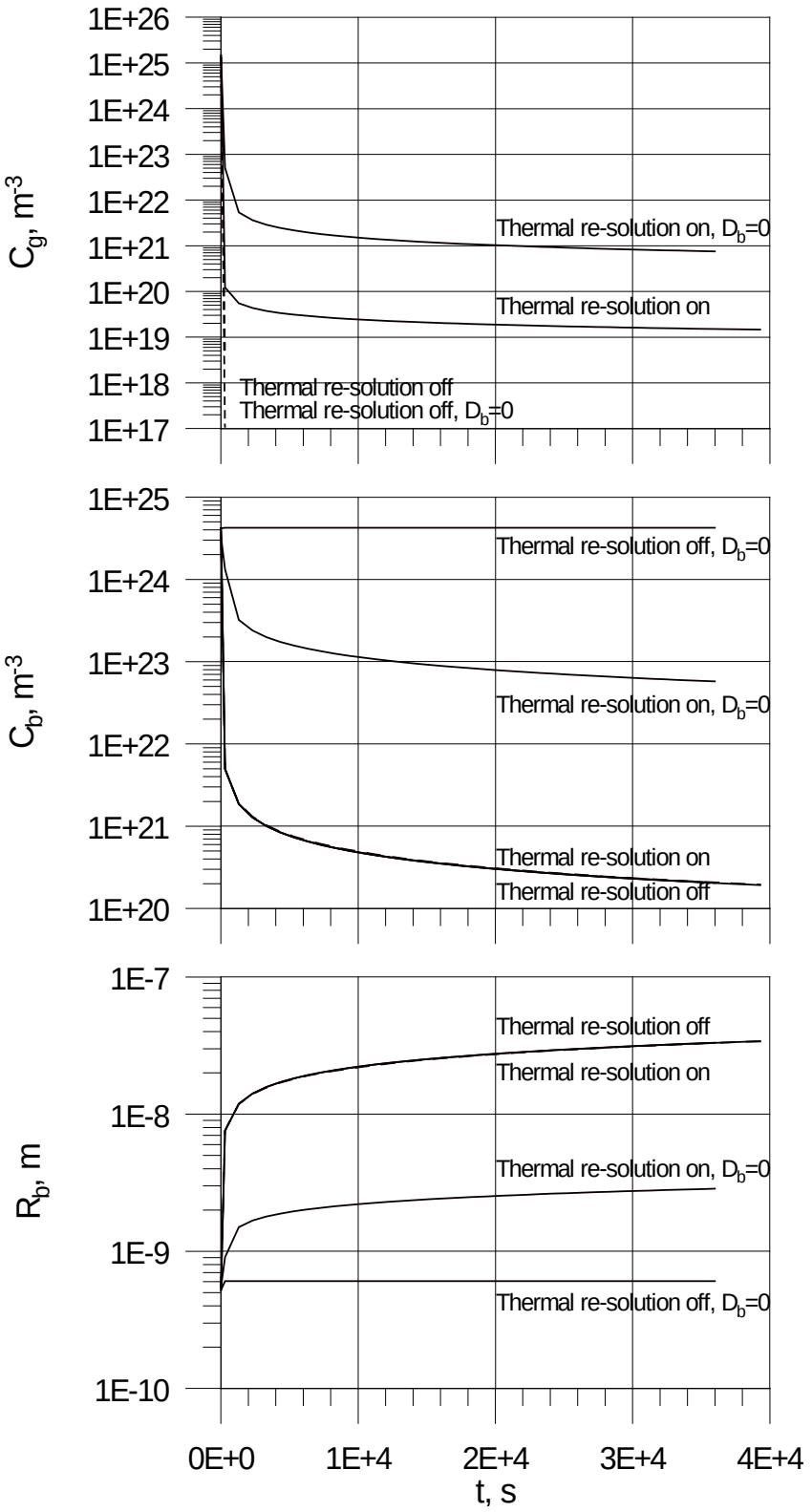

Fig. 5.5. The model simulations of the bubble system behaviour during annealing at high temperature.

Irradiation ($2 \cdot 10^7$ s): T = 1400 K, F = 10^{19} $m^{-3}s^{-1}$. Annealing: T=2500 K.

6. Gas release during post-irradiation annealing

A rapid growth of the intragranular bubbles owing to the gas atoms diffusion from the solid matrix is usually observed during high temperature annealing of irradiated fuel [29, 33]. A noticeable decrease (by several orders of magnitude) of the bubble number density occurs simultaneously with the bubble size increase (up to hundreds nm at high annealing temperatures). This process of the bubble number decrease is usually associated with the Brownian motion of the bubbles leading to their coalescence (via direct collisions) into larger ones in the grain bulk and transport to the grain boundaries. However, evaluation of the experimental data by the MFPR code shows that a rather low mobility of the bubbles at T ≤ 1800°C measured in [13] does not allow a correct description of the bubble system evolution. Even additional assumptions on the bubble diffusivity increase up to values determined by the surface diffusion (i.e. by several orders of magnitude) during annealing (e.g. recommended in [39]), slightly improve the description, however, does not allow a satisfactory agreement with measurements of gas release and bubble coalescence. A complementary mechanism of bubble growth under annealing conditions associated with the thermal re-solution effects considered in various papers [1, 31, 35, 36], turns out to be also too weak, as demonstrated in Section 5.

As shown in the previous paper [1], in the absence of irradiation ($K \to 0$ in Eq. (2.1)) in the annealing stage, the subsystem of point defects (vacancies and interstitials) rather quickly attains its equilibrium state ($c_{v,i} = c_{v,i}^{eq}$). For instance, this relaxation time at the annealing temperature 1500°C can be estimated from Eq. (2.1) as $\tau_{eq} \sim (D_v k_v^2)^{-1} \approx 10^{-1}$ - 10^{-2} s, where $D_v \approx 10^{-9}$ - 10^{-10} cm^2/s is the thermal value of the vacancy diffusion coefficient. A more slow process of the bubble growth occurs owing to the gas atom and point defect diffusional transport to bubbles. Since $D_g c_g << D_u$, where $D_u \approx 10^{-16}$ - 10^{-15} cm^2/s is the thermal value of the uranium self-diffusion coefficient, the gas transport determines the bubble growth rate during the initial period of the annealing stage. Despite a relative slowness of this process (in comparison with thermalisation of point defects), sinking of gas atoms into bubbles occur during a few minutes or seconds at high temperatures. Hence, under annealing conditions at 1500°C, the characteristic time τ_s of diffusional sinking of gas atoms into bubbles is estimated as $\tau_s \sim (D_g k_v^2)^{-1} \approx 10^2$ s; after this time practically all gas atoms are captured by bubbles, and gas transport to grain boundaries and the subsequent release can be provided only by bubbles.

During bubbles growth and coalescence, extended defects such as dislocation loops uniformly distributed in the grain bulk, serve as the main source for vacancies (necessary for the bubble equilibration) and afford the equilibrium concentration of the point defects in the crystal bulk. This may explain the observed dislocation creep and enhanced bubble growth by dislocation sweeping under annealing conditions [17]. However, a strong pinning of dislocations by the swept bubbles very quickly saturates this source of point defects, and grain boundaries apparently becomes the dominant source of vacancies during the most period of the annealing tests. In this situation a vacancy flux directed from grain surface to its interior arises that increases bubble migration along the vacancy gradient in the opposite direction, as proposed recently by Evans [40].

Strictly speaking, a mechanism of bubble migration to the grain boundaries along the vacancy gradient was initially analysed and described in [41] and [42]. Later Evans proposed to apply a similar mechanism to the description of the enhanced gas release at annealing. However, in his paper [41] he did not present any quantitative calculations, but restricted himself by a qualitative consideration of the phenomenon.

In order to handle this problem quantitatively, a simple analytical model is developed in the present section. This model allows not only to explain a continuous increase of gas release during the annealing stage, but also to relate it to the accompanying phenomenon of considerable bubble coalescence and swelling observed in the annealing tests [5, 43, 44].

6.1. Model description

In order to simplify modelling, a homogeneous space distribution of equal-size bubbles in the grain is considered. These simplifications allow analytical treatment of the problem, however, might be easily avoided after implementation of a more realistic model in the MFPR code (foreseen for the future code development).

As above explained, after some initial period of the annealing stage, grain boundaries become the main source of vacancies and for this reason, vacancy flux from boundaries to grain interior appears. In accordance with the model predictions [40] and [41], bubble flux in the opposite direction arises. Since (as above explained) gas atoms sinking into the bubbles is a relatively quick process which occurs during the initial 10^2–10^3 s of the annealing stage, in a late stage of annealing bubble coalescence determines vacancy deficit in the grain bulk and corresponding vacancy flux from the boundaries. For this reason, the proposed model self-consistently accounts for both processes of gas release and bubble coalescence (swelling) observed in the annealing tests.

In accordance with [41], the bubble velocity $\vec{v}$ in the gradient of vacancy concentration c_v is determined by the relationship:

$$\vec{v} = 2D_v \vec{\nabla} c_v \,, \tag{6.1}$$

where D_v and c_v are the uranium vacancy diffusion coefficient and bulk concentration (number of vacancies per U atom) in the UO_2 matrix, respectively.

Correspondingly, gas atom flux $\vec{J}_g$ to the grain boundary via bubble migration, takes the form:

$$\vec{J}_g = \rho_b \vec{v} N_b \,, \tag{6.2}$$

where $\rho_b(t)$ is the bubble number density and $N_b(t)$ is the number of gas atoms in a bubble, both being spatially homogeneous in accordance with the above accepted model simplification.

As above explained, practically all gas atoms were captured by bubbles within a relatively short initial period of the annealing stage, and for this reason, neglecting an amount of gas atoms on the boundaries in comparison with the bulk content, the total gas content N_g in the spherical grain with the radius R_g takes the form:

$$N_g \approx \rho_b N_b (4\pi/3) R_g^3 \,, \tag{6.3}$$

and its variation with time is determined by the gas flux, Eq. (6.2) at the grain surface:

$$-\frac{dN_g}{dt} = J_g(R_g) 4\pi R_g^2 \,. \tag{6.4}$$

After substitution of Eqs. (6.1–3) in Eq. (6.4), one gets:

$$-\frac{dN_g}{dt} = \frac{6 N_g D_v \nabla c_v(R_g)}{R_g} \,. \tag{6.5}$$

On the other hand, the diffusion vacancy flux at the grain boundary $D_v \nabla c_v(R_g)$ determines time variation of the total volume of intragranular bubbles due to their coalescence and subsequent equilibration:

$$\frac{d(4\pi R_b^3 \rho_b)}{3dt} = \frac{3 D_v \nabla c_v(R_g)}{R_g} \,. \tag{6.6}$$

For large enough bubbles (with radius $R_b \geq 5$ nm that is attained rather quickly in the initial stage of annealing) obeying the ideal gas law, the equilibrium condition takes the form:

$$\frac{4\pi R_b^3}{3} \frac{2\gamma}{R_b} = kTN_b \,. \tag{6.7}$$

Substitution of Eqs. (6.6) and (6.7) in Eq. (6.5) finally yields:

$$-\frac{dN_g}{dt} = \frac{kT}{\gamma}\frac{3N_g}{4\pi R_g^3}\frac{d}{dt}(N_g R_b)\,. \tag{6.8}$$

The analytical solution of Eq. (6.8) has the form:

$$AN_g R_b = \ln(B/N_g)\,, \tag{6.9}$$

where $A = \frac{kT}{\gamma}\frac{3}{4\pi R_g^3}$ and B is the integration constant.

If one designates the initial values at $t = t_0$ as $R_b = R_0$ and $N_g = N_0$, then $\ln(B) = AN_0R_0 + \ln(N_0)$, and Eq. (6.9) takes the form:

$$N_g R_b = N_0 R_0 + A^{-1}\ln(N_0/N_g)\,. \tag{6.10}$$

This solution can be simplified, until $\Delta N = N_0 - N_g << N_0$:

$$\frac{\Delta N}{N_0} \approx \frac{AN_0(R_b - R_0)}{AN_0R_b + 1}\,. \tag{6.11}$$

It can be generally considered that $R_b >> R_0$, since the bubble radius increases by orders of magnitude in the annealing tests. The term AN_0R_b can be evaluated as:

$$AN_0R_b \approx 0.2N_0\frac{R_b}{a}\frac{3\Omega}{4\pi R_g^3} = 0.2\frac{R_b}{a}\frac{N_0}{N_U}\,, \tag{6.12}$$

where $a \approx 0.3$ nm is the UO_2 lattice constant and N_U is the number of uranium atoms in the grain. Therefore, under conditions of the Baker and Kileen's tests [43] with irradiation burnup ≈ 4 at.% (i.e. $N_0/N_U \approx 10^{-2}$), one obtains $AN_0R_b << 1$ until $R_b << 100$ nm, and from Eq. (6.11) $\Delta N/N_0 \approx AN_0R_b$, i.e. gas release smoothly increase along with the bubble radius growth. When R_b attains ~ 100 nm, $\Delta N/N_0$ is not anymore small, and starts to approach to 1 (i.e. gas release $\rightarrow$ 100%) when $R_b >> 100$ nm, this is in agreement with observations [43].

6.2. Model validation

An exact numerical solution of Eq. (6.9) is presented in Fig. 6.7 where the initial time moment t_0 corresponds to the onset of the annealing stage; respectively, R_0 is chosen as 1 nm (i.e. a typical value for the bubble radius at the end of irradiation stage). This allows a direct comparison with experimental data of Baker and Kileen's tests [43] obtained at 1600°C in three various time moments. These results well confirm the above presented estimations, and additionally demonstrate that the model is able to correctly describe the whole annealing stage, if the time evolution of the bubbles radius will be correctly predicted by the code.

Therefore, the obtained Eq. (6.11) qualitatively correctly describes the observed correlation between gas release and kinetics of bubble coalescence in the annealing tests.

6.3. Discussion

It is important to note that the current version of MFPR significantly underestimates (for the above presented reasons) bubble growth due to coalescence in the annealing stage, and for this reason one might expect underestimation of the predicted by Eq. (6.11) gas release. However, implementation of the new model in the code will additionally lead to a significant intensification of *the bubble coalescence due to biased migration in the above considered vacancy gradient*. In its turn, this will lead to the subsequent increase of gas release. Therefore, a self-consistent consideration of both processes (bubble migration and coalescence) in the vacancy

gradient during annealing stage may eventually lead to a quantitative agreement of the code predictions with observations [5, 43, 44]. This task is foreseen for the future development of the code.

6.4. Conclusions

A simple analytical model that accounts for the biased migration of bubbles in the vacancy gradient that occurs under annealing conditions due to bubbles growth and coalescence, is developed. This model allows not only to explain a continuous increase of gas release during the annealing stage, but also to relate it quantitatively to the kinetics of bubble coalescence and swelling, in agreement with measurements in the annealing tests.

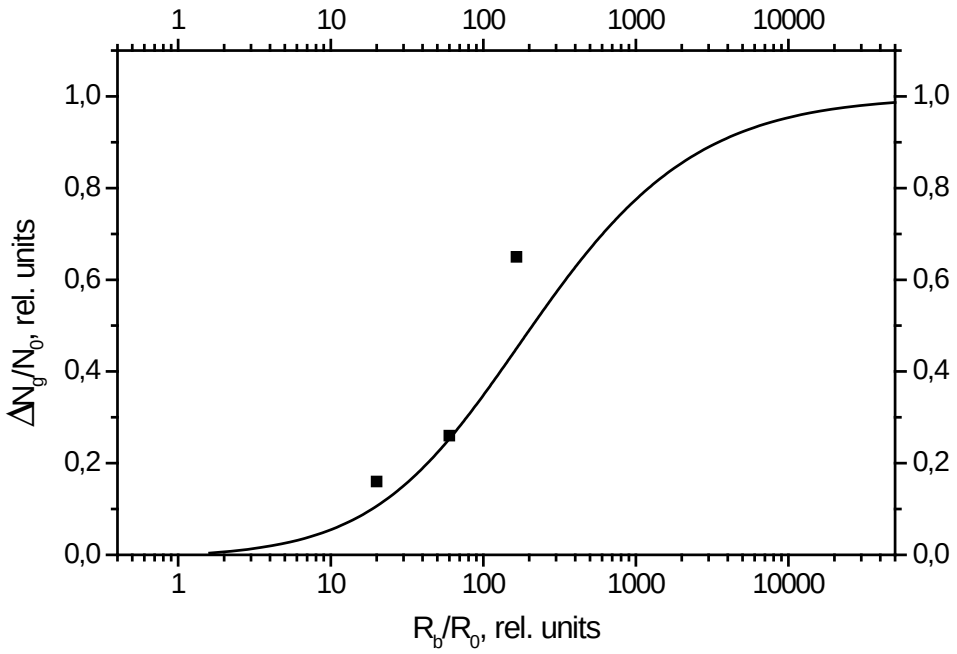

Fig. 6.7. Model prediction of gas release dependence on mean bubble radius during annealing stage, in comparison with experimental observations [43] at 1600 ℃ in three various moments (50 s, 1.4 h, 24 h)

7. General conclusions

In order to improve the microscopic description of the fission gas behaviour, the new models (initially considered in [1]) were further developed and implemented in the mechanistic code MFPR. The models treat irradiation and thermal re-solution effects on intra- and intergranular bubbles under various conditions of UO_2 fuel operation: steady-state irradiation, transient and post-irradiation annealing. Implementation of the developed models in the MFPR code allowed a significant improvement of code predictions with respect to gas release and fuel swelling.

After validation of the advanced version of the MFPR code with the newly implemented models, the following specific conclusions were derived:

- ☐ The new model that accounts for the irradiation induced limitation on the bubble sink strength at T < 1500 °C under steady irradiation conditions, allows a satisfactory prediction of a complicated non-monotonous behaviour of intragranular bubbles at a late stage of irradiation observed in recent tests with high burn-up fuel.

- ☐ The new model for self-consistent consideration of the irradiation induced re-solution of gas atoms from bubbles, allows to avoid (or to reduce) non-physical tuning of the code parameters (i.e. bubble diffusivity) and to attain a reasonable prediction for microscopic observations (i.e. bubble size distribution) in the transient tests.
- ☐ The new model for the irradiation effects on grain face bubbles based on the self-consistent consideration of diffusion and re-solution processes in the grain and grain faces, reveals an important role of grain boundary diffusion of gas atoms to edges before interlinking of intergranular bubbles, and allows a satisfactory agreement of the code predictions with measurements for gas release from irradiated fuel. Calculations of the intergranular bubbles growth kinetics are also in a fair agreement with the grain face microstructure observations.
- ☐ The new model for thermal re-solution of gas atoms from bubbles at high temperatures based on the self-consistent consideration of non-ideal gas corrections to the gas state law (in the Van-der-Waals or hard spheres approximation) in small bubbles and to the solubility of gas atoms in the solid matrix in equilibrium with the gas phase at a given pressure (Henry's law), confirmed that the thermal re-solution process determines the onset of bubble formation under steady irradiation conditions. Namely, the new model predicts a complete suppression of the bubble nucleation process at $T > 2000°C$, and a significant delay in the onset of the bubble formation at low temperatures $T < 800°C$, in a qualitative agreement with observations.
- ☐ The simple analytical model that accounts for the biased migration of bubbles in the vacancy gradient that occurs under annealing conditions due to bubbles growth and coalescence, allows to quantitatively relate gas release to the kinetics of intragranular bubble coalescence and swelling, in agreement with measurements in the annealing tests.

Acknowledgements

The authors thank Dr. V. Ozrin and Ms. V. Kulik for valuable discussions and comments. This work was supported by IPSN, Cadarache (France) under the Contract No. 4000 A 109310 on the mechanistic code MFPR development; the personal interest and support of Dr. M. Kissane (IPSN) is acknowledged.

References

1. M.S. Veshchunov, J. Nucl. Mater., 277 (2000) 67.
2. A.V. Berdyshev, R.R. Galimov, V.D. Ozrin, A.V. Palagin, V.E. Shestak, M.S. Veshchunov, "MFPR version 1.1 revision 1 module. User manual", - Note Technique SEMAR 99/55, IPSN-CEA, Cadarache, France, 1999.
3. A.D. Brailsford, R. Bullough, Philosophical Transactions of the Royal Society, A302 (1981) 87.
4. R.J. White, M.O. Tucker, J. Nucl. Mater., 118 (1983) 1.
5. S. Kashibe, K. Une, K. Nogita, J. Nucl. Mater., 206 (1993) 22.
6. K. Nogita, K. Une, Nucl. Instrum. Meth. Phys. Res., B91 (1994) 301.
7. J. Rest, G.L. Hofman, J. Nucl. Mater., 277 (2000) 231.
8. R.S. Nelson, J. Nucl. Mater., 31 (1969) 153.
9. J.A. Turnbull, J. Nucl. Mater., 50 (1974) 62.
10. C. Baker, J. Nucl. Mater., 71 (1977) 117.
11. I.L.F. Ray, H. Thiele, Hj. Matzke, , J. Nucl. Mater., 188 (1992) 90.
12. P. Knudsen, C. Bagger, H. Carlsen, I. Misfeldt, M. Mogensen, Nucl.Technol., 72 (1986) 258.
13. W. Beere, G.L. Reynolds, J. Nucl. Mater., 47 (1973) 51.

14. C.C. Dollins, F.A. Nichols, J. Nucl. Mater., 91 (1976) 143.

15. T.J. Heames, D.A. Williams, N.E. Bixler, A.J. Grimley, C.J. Wheatley, N.A. Johns, P. Domogala, L.W Dickson, C.A. Alexande, I. Osborn-Lee, S. Zawadzki, J. Rest, A. Mason, R.Y. Lee, VICTORIA: A Mechanistic Model of Radionuclide Behaviour in the Reactor Coolant System under Severe Accident Conditions,- NUREG/CR-5545, 1992.

16. I.J. Hastings, J. Nucl. Mater., 54 (1974) 138.

17. K. Une, S. Kashibe, J. Nucl. Sci. Technol., 27 (1990) 1002.

18. S. Kashibe, K. Une, J. Nucl. Sci. Technol., 28 (1991) 1090.

19. J.A. Turnbull, M.O. Tucker, Philos. Mag., 30 (1974) 47.

20. M.H. Wood, J. Nucl. Mater., 119 (1983) 67.

21. J.R. Matthews, M.H. Wood, J. Nucl. Mater., 91 (1980) 241.

22. M.V. Speight, Nucl. Sci. Engrg., 37 (1969) 180.

23. P. Van Uffelen, SCK-CEN Report, 1998.

24. G.B. Alcock, R.J. Hawkins, A.W.D. Hills, P. McNamara, Paper SM-66/36, IAEA, Symp. Thermodynamics, Vienna, 1965, p. 57.

25. M.O. Tucker, J. Nucl. Mater., 89 (1979) 199.

26. S.R. Pati, M.J. Dapt, D.R. O'Boyle, J. Nucl. Mater., 50 (1974) 227.

27. C.T. Walker, P. Knappik, M. Mogensen, J. Nucl. Mater., 160 (1988) 10.

28. H. Zimmermann, J. Nucl. Mater., 75 (1978) 154.

29. C.Baker, J. Nucl. Mater., 66 (1977) 283.

30. J.A. Turnbull, J. Nucl. Mater., 38 (1971) 203.

31. D.A. MacInnes, I.R Brearley, J. Nucl. Mater., 107 (1982) 123.

32. I.R Brearley, D.A. MacInnes, J. Nucl. Mater., 118 (1983) 68.

33. K.C. Russell, Acta Metall., 26 (1978) 1615.

34. C.A. Parker, K.C. Russell, Scripta Met. 15 (1981) 643.

35. I.R Brearley, D.A. MacInnes, J. Nucl. Mater., 118 (1983) 68.

36. P.T.Elton et al., J. Nucl. Mater., 135 (1985) 63.

37. J.A. Turnbull, R.M. Cornell, J. Nucl. Mater., 36 (1970) 161.

38. M.S.Veshchunov, Development of the Theory of Fission Gas Bubble Evolution in Irradiated UO_2 Fuel, - Preprint IBRAE-98-11, Moscow, 1998.

39. J. Rest, S.A. Zawadzki, FASTGRASS: A Mechanistic Model for the Prediction of Xe, I, Cs, Te, Ba, and Sr Release from Nuclear Fuel under Normal and Severe-Accident Conditions, NUREG/CR-5840, ANL-92/3, 1992.

40. J.H. Evans, J. Nucl. Mater., 246 (1997) 121.

41. Ya.E. Geguzin, M.A. Krivoglaz, "Migration of Macroscopic Precipitates in Solid Materials", Moscow, 1971 (in Russian).

42. F.A. Nichols, Acta Met., 20 (1972) 207.

43. C. Baker, C. Kileen, "Fission gas release during post irradiation annealing of UO_2", Materials for nuclear reactor core applications, BNES, London, 1987, Paper 24, p.183.

44. I. Zacharie, S. Lansiart, P. Combette, M. Trotabas, M. Coster, M. Groos, J. Nucl. Mater., 255(1998)85-91.